3

CONTROLLED PYROLYSIS OF METAL-CONTAINING PRECURSORS AS A WAY FOR SYNTHESIS OF METALLOPOLYMER NANOCOMPOSITES

A. D. Pomogailo, A. S. Rozenberg, and G. I. Dzhardimalieva

Institute of Problems of Chemical Physics, Russian Academy of Sciences, Chernogolovka Moscow Region, Russia

The processes of thermal decomposition play an important role in various practical fields including metallurgy, mineral conversion processes, pyrogenic chemical technology, pyrolysis and thermal treatment of wood and coal, combustion of natural and synthetical fuels, coal carbonization, the prevention of grain spontaneous ignition, and so on. There is still a need for scientifically well-founded approaches to control the thermal decomposition of materials. Many studies focus attention on the chemical transformations and reactions in the pyrolized systems and on the creation of mathematical models of such processes as the major parts of the theory of chemical decomposition of complex substances.

Thermolysis is widely used in the synthesis of nano-sized metallopolymer composites. This is a result of the specifics of the preparation of such materials. In spite of a variety of the methods for the preparation of metallopolymer nanocomposites, there are two principal routes: "bottom-up" and "top-down."

Metal-Polymer Nanocomposites, Edited by Luigi Nicolais and Gianfranco Carotenuto
ISBN 0-471-47131-3

Widely spread bottom-up processes consist of nanoparticle assembling from the separate atoms or ions by means of their reduction in the presence of a polymer matrix (or its precursor). Such a process can be represented by the following stages [1]:

A chain generation (the stage of the M_1 active particle formation)

$$M \xrightarrow{k_0} M_1 + M_j \tag{1}$$

A chain (cluster) growth

$$M_j + M \xrightarrow{k_j} M_{j+1} \qquad (1 < j < \infty) \tag{2}$$

Formation of the products (P, P*)

$$M + M_j = M_1 + P^* \tag{3}$$

From the viewpoint of kinetics, all these reactions can be considered as a chain process. In the general case, the bottom-up processes can be carried out by "wetting" and "drying" means. For the former, at least, one of the components (or, at least, on some stage of the multistage process) should be used as a solution or a dispersion in solvent. The "drying" method allows us to exclude totally the solvent from the technology. Due to a low solubility of components and, in some cases, their chemical instability in solution as well as the difficulties in removing a solvent (including the ecological reasons), the drying processes are more preferable for synthesis of metallopolymer nanocomposites. However, the number of such methods is limited, and technologically final adjustment methods are quite rare.

One such potential method can be pyrolysis—a new and rapidly developing field in the nanocomposites science. This route consists of a controlled pyrolysis of metallopolymers, organic and nonorganic acid salts, metal complexes, and metal-containing compounds in the presence of polymers. Such processes can be carried out into a gaseous phase (the different variants of the CVD, CVD synthesis), liquids (in high-temperature solvents, in the suspension decomposition products from the high-molecular-weight liquids or polymer melts [2]). Of great interest is the thermal decomposition in the solid state (in vacuum or in a self-generating atmosphere of the gaseous transformation products). The processes temperature can be kept constant (isothermal conditions) or be program-controlled (nonisothermal conditions, thermal analysis mode). The processes rate can be controlled by the evolving gaseous product amounts, the change of the initial or final products, or the spectral and magnetic properties of the reacting system as a whole. Below we will consider the thermolysis of the most common precursors, namely, metal-containing polymers, the high-

volatile metal-forming compounds such as metal carbonyls ($M_a(CO)_b$) and carbonitrosyls ($M(CO)_x(NO)_y$), formates, acetates, and some π-allyl complexes. Naturally the metal-containing monomers are of special interest, as is the computer modeling of such processes.

1. METAL-CONTAINING POLYMERS AND THEIR THERMAL DECOMPOSITION

There are three main methods for synthesis of metal-containing polymers. Their spreading degree can be divided as follows: interaction of metal compounds (MX_n) with linear functionalized polymers when a backbone has not been affected (polymer-analogous transformations, method A); preparation of metallopolymers by a condensation of appropriated precursors; in this case the metal ion is embedded into a main polymer chain, and its removal is accompanied by a total rupture of the chain (method B); and, finally, a recently developed method, namely, polymerization and copolymerization of metal-containing monomers (method C). The method of synthesis of metal-containing polymers seems to significantly affect their properties. For example, in method A not all functional groups of polymer participate in the complexation, and remaining vacant groups alter the properties of the metallopolymer formed. In method B each unit of polymer contains an equivalent of chelate-bonded metal. Such polymers are known to be stable up to 520–720 K, and some of them even up to 900 K [3]. The thermal transformations of metallopolymers of the condensation type are well-studied because there was a need to obtain thermostable polymers. At the same time, the investigations of thermolysis of carbon-chain polymers (A and C) are limited, although the considerable efforts in this area have been undertaken [4–9].

Kinetics of thermal decomposition of such polymers can be described by the equation for one-stage chemical reaction [10]:

$$dw/dt = k(w - w_r)^n, \qquad k = k_0 e^{-E/RT} \tag{4}$$

where k_0 is the preexponential coefficient; E is the energy of activation; n is the reaction order; $w = M/M_0$, $w_r = M_r/M_0$; M_r, is the mass of the residue nondecomposed at the temperature of experiment, and M_0 and M are the initial and current mass of the sample, respectively; w_r is the member taking into account the nondecomposed solid residue of polymer.

As a rule, the complexation of the initial precursors with functional groups of polymer precedes the formation of metallocomposites [11]. Essentially, the macromolecular complex formed undergoes thermolysis. For a long time the Pt and Pd colloids were known to be stable to heating [12]. The parameters of

thermal decomposition depend on the thermostability of the polymer itself, on the stability of the macromolecular complex formed, on the intermolecular interaction, which diminishes with temperature, and on the heating temperature. It should be noted that the formation of macrocomplex itself can lead to a partial destruction of polymer. For example [13], this is possible due to a rupture of polymethylmethacrylate chains under the influence of the mechanical forces, namely, from the tensile stresses (σ) occurring at the formation of the complex:

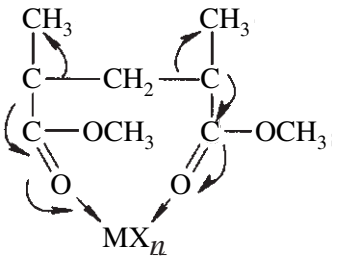

Scheme 3.1.

The tension leads to a decrease of the C–C bond energy to the value $E = E_0 - \gamma\sigma$, where γ is the structure coefficient determining the distribution of tensile stresses in the bonds (see reference 14). Not only the tensile stress, but also the energy of the M–O bond and the conformation of the cyclic complex, is important because a local stress of C–C bonds diminishes the potential barrier of their rupture. A mutual effect of the tensile stress and thermal motion have been analyzed in reference 15.

In principal, to describe the thermal destruction of polymer chains the mathematical models [16], which take into account the differences between the rates of decomposition of "complexed" (N_z) and free (N_f) chain units, can be used:

$$dc/d\tau = k_1 N_z + k_2 N_f \tag{5}$$

where k_1 and k_2 are the constants of the reaction rate of decomposition of the chain units bonded with MX_n and free ones, respectively. However, there is no still such analysis. The transformations are considerably more complicated for the thermolyzed polymer composites containing metal halogenides, such as the systems MX_n – PMMA (M = Cr, Mn, Zn; X = Cl, Br) [17]. For example, the $CrCl_3$–PMMA composite lost under pyrolysis at 523–773 K is about 62% in mass. The volatile fraction contains monomer, carbon oxides, HCl, methane

traces, and nonidentified organic products (in the condensed phase along with nonsaturated oligomers, the highly dispersed solid chromium anhydride and oxides are present [18–22]. A quantitatively similar picture of PMMA destruction was observed (at 373–873 K) for $MnCl_2$ [23] when one of the final solid pyrolysis products is manganese oxide formed during the PMMA manganese ionomer thermolysis. The compound $CuBr_2$ (in concentrations of 5–10%) has a thermostabilizing effect for PEO [24].

The metallopolymeric systems pyrolysis permits us to produce some other important and interesting products. For example, the carbon films, containing cobalt nanoparticles, can be produced by a pyrolysis of macrocomplex ($CoCl_2$ with PAN) at 1570 K [25]. The thermotreated PAN complexes with copper halogenides has an electrical conductivity [26], and the macrocomplexes containing two metals (e.g., Co, Ni, or Rh) demonstrates a synergy in thermostabilization [27]. The Fe, Co, and Ni nanoparticles can be used as catalysts for a low-temperature graphitization of amorphous carbon [28]. Such examples are very numerous and demonstrate that metal acetylacetonates in polymer matrices can perform a double function; that is, along with their decay that leads to the formation of metal-containing nanoparticles, they interact with the matrix, initiating its depolymerization and destruction [29].

Such investigations are numerous including those concerning macromolecular π-complexes, but most of them provide only qualitative information. Here let's only note that the products of thermal decomposition of metal salts in polymer matrices are usually highly dispersed metal oxide particles. Their size is determined by the competition between thermolysis and sintering. A decrease in the probability of sintering can be attained by a fast decomposition of salts at the high temperatures followed by cooling of the products formed [30].

2. THE PECULIARITIES OF THERMOLYSIS OF TRANSITION METAL POLYACRYLATES

The pyrolysis of transition metal carboxylates (in the example of Ni^{2+}) has an essential place due to both (a) the quantitative characteristics of the main stages and (b) the properties of the products obtained. Such metallopolymers can be prepared by two principally different routes: by the above-mentioned polymer-analogous reactions, namely, by the interaction of polyacrylic acid with metal salts Ni^{2+}, (PAA-Ni^{2+}), Co^{2+}, Fe^{3+}, and so on (method A), or by radical polymerization of the appropriated monomers—for example, nickel acrylate, $[Ni(CH_2CHCOO)_2]_n$, to give nickel polyacrylate (NiPAcr) (method C). The kinetic peculiarities of metallopolymers thermolysis were compared with the behavior of their low-molecular-weight analogues: nickel propionate,

$Ni(CH_3CH_2COO)_2 \cdot 2H_2O$ $Ni(Prop)_2$, and acrylate, $Ni(CH_2CHCOO)_2 \cdot 2H_2O$ $Ni(Acr)_2$. The synthesis and characterization of such products are given in reference 4.

Let us consider the kinetic behavior of PAA–Ni^{2+} and NiPAcr at their thermolysis. It is known that carboxyl groups of PAA, as well as their low-molecular-weight analogues, are able to chemically bond transition metal compounds. The polymer containing a number of functional groups is a polydentate ligand. This defines its behavior in the complexation reaction. Thus, using various physicochemical methods, it was shown [31] that the interaction of $Ni(CH_3COO)_2$ with PAA is an equilibrium and reversible reaction, it being known the equilibrium is attained immediately after mixing of the components. It was found there are both a "single-point" binding of Ni(II) (the C_1 form) and the Ni(II) binding with two units of the same (the C_2 form) or two different (C_3) polymer chains. The general scheme of such a reaction can be represented as follows:

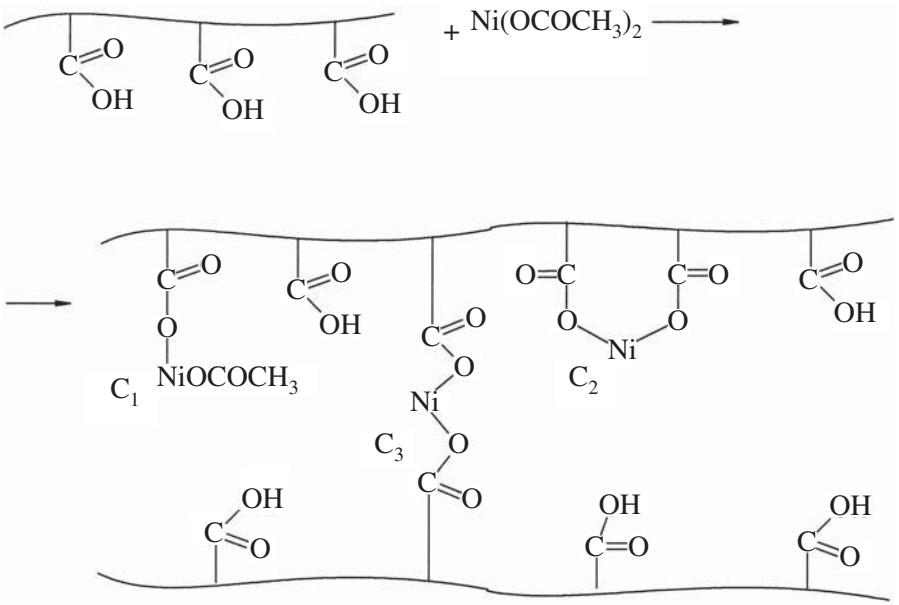

Scheme 3.2.

As a rule, the content of the C_1 form is an order of magnitude less than that for C_2; in the polymer the intramolecular cyclization usually takes place. The portion of Ni(II) ions that binds two chains (the form C_3) is quite small. The complexation reactions with macromolecular ligands are appreciably influ-

enced by a cooperative character of the process—that is, the dependence of reactivity of macroligand functional groups on the state of another units [32]. In particular, for this reason (so called "the effect of neighbor") many carboxylic groups of macroligand do not bind Ni(II) ions. Their portion in the system considered is about 0.3. At the same time for nickel polyacrylate, each unit of the chain contains an equivalent of Ni^{2+}; that is, there is no the vacant carboxylic groups. Such a polymer chain is strongly strained. Thermal transformations of the compound considered are accompanied by gas evolution. The kinetics of gas evolution was recorded using a membrane zero-manometer (Figure 3.1). The kinetic parameters of the process are given in Table 3.1. The kinetics of gas evolution depends on T_{exp}. The change of the m_0/V ratio (at constant T_{exp}), where m_0 is the mass of sample and V is the volume of a reaction vessel, practically does not affect the rate of gas evolution. The character of conversion $\eta(t)$ depends on the nature of metallopolymers and is satisfactorily approximated by the following types of integral equations (here $\eta = (\alpha_{\Sigma,t} - \alpha_{\Sigma,0})/(\alpha_{\Sigma,f} - \alpha_{\Sigma,0})$ is the degree of conversion; $\alpha_{\Sigma,0}$, $\alpha_{\Sigma,t}$, and $\alpha_{\Sigma,f}$ are the mole amounts of

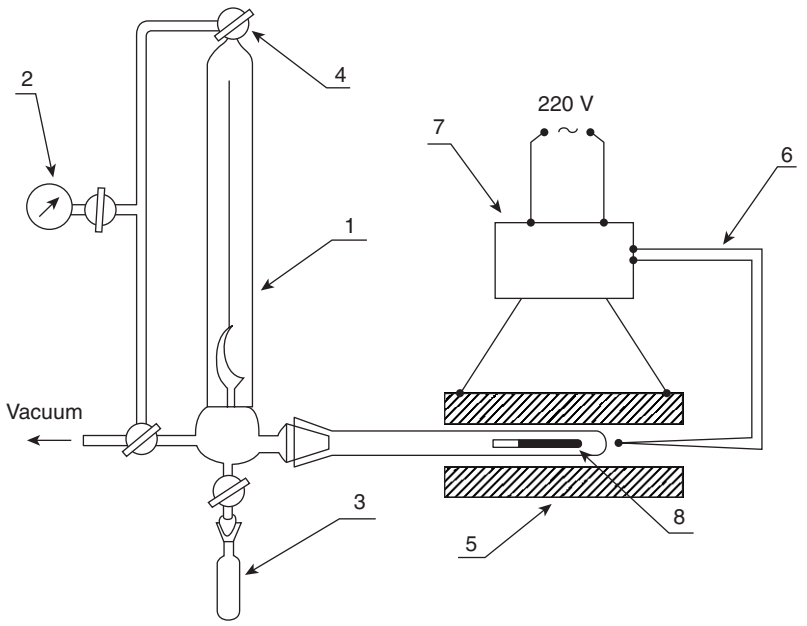

Figure 3.1. A schema of the apparatus for the kinetic investigation of the gas evolution. 1, the reaction vessel; 2, vacuum gage; 3, gutters for sampling of the gaseous products; 4, vacuum cocks; 5, the heating furnace with rectangular profiles of temperatures, high-temperature thermocouple; 7, thermoregulator; 8, ampule with sample.

TABLE 3.1. The Dependence of Kinetic Parameters on the Temperature of Thermolysis of Ni-Containing Precursors

			η_∞, $\alpha_{\Sigma,f} = A \exp[-\Delta H/(RT)]$			k, $\xi_0 = A \exp[-E_a/(RT)]$	
Compound	T_{exp} (K)	η_∞, $\alpha_{\Sigma,f}$	A, sec^{-1}	ΔH (kJ/mole)	k_i, ξ_0	A, sec^{-1}	E_a (kJ/mole)
$NiAcr_2$[a]	573–633	η_∞	2.6	4.6	k_1	1.7×10^{17}	242.5
					k_2	7.5×10^{8}	156.8
NiPAcr	563–598	$1 - \eta_\infty$	1.45×10^{-6}	–61.9	k_1	4.5×10^{8}	143.0
					ξ_{01}	7.1×10^{11}	151.7
					k_2	5.9×10^{5}	107.0
					ξ_{02}	$(3.2 \pm 0.3) \times 10^{-2}$ ≈ const	
PAA-Ni^{2+}	573–643	$\alpha_{\Sigma,f}$	5.38×10^{3}	39.3	k_1	2.1×10^{5}	87.8
					ξ_0	8.1×10^{5}	81.5
Fe_2NiAcr_9[b]	603–643	η_∞	4.4×10^{7}	96.1	k_1	6.1×10^{6}	129.6
					k_2	0.6×10^{2}	79.4
$Ni(Prop)_2$	603–643	$\alpha_{\Sigma,f}$	0.32×10^{2}	16.7	k_1	3.1×10^{8}	117.0

[a] η_∞ are in the range of 0.29 (573 K) to 0.69 (633 K).
[b] η_∞ are in the range of 0.34 (603 K) to 1.0 (643 K).

gaseous products evolved per mole of the initial compound in the beginning, at the moment of t, and in the end of gas evolution, respectively). Thermolysis of the polymer PAA–Ni^{2+} (obtained by method A) is described by the equation for the rate of an autocatalytic reaction of the first order:

$$\eta(t) = \xi_0\left(e^{k1t} - 1\right)\left(1 + \xi_0 e^{k1t}\right)^{-1} \tag{6}$$

The kinetics of thermolysis of NiPAcr (obtained by radical polymerization of nickel acrylate (method B) reveal the more complex picture (Figure 3.2).

At a small degree of conversion the $\eta(t)$ dependence is autocatalytic and is satisfactorily described by equation (6). In the region of low T_{exp} (at the constant m_0/V) the $\eta(t)$ dependence reaches the maximum value of $\eta_{max}(t)$ and then in the end of gas evolution falls to η_∞.[1] This equation is true up to $t \approx \tau$ when the experimental curves of $\eta(t)$ begin to deviate from equation (6). At $t > \tau$ the $\eta(t)$ is transformed into an expression approximated by the equation

$$\eta(t) = \xi_{01}\left(e^{k1t} - 1\right)\left(1 + \xi_{01} e^{k1t}\right)^{-1} - (1 - \eta_\infty)\xi_{02}\left(e^{k2t} - 1\right)\left(1 + \xi_{02} e^{k2t}\right)^{-1} \tag{7}$$

[1] Here $\eta(t) = 0.5(\alpha_{\Sigma,t} - \alpha_{\Sigma,0})/(\alpha_{\Sigma,f} - \alpha_{\Sigma,0})$.

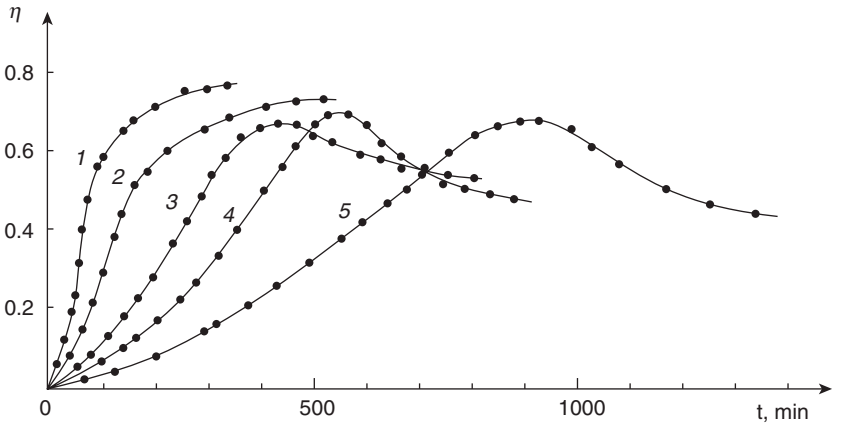

Figure 3.2. The influence of T_{exp} on the η(*t*) dependence during thermal transformation of NiPAcr at the constant ratio $(m_0/V) \times 10^3 = 2.09\,g \cdot cm^{-3}$: 1, 598; 2, 593; 3, 583; 4, 573; 5, 563 K. Solid line, calculated data; dots, the experimental data.

Taking into account that $\tau \approx 1/k_1$ and $\alpha_\Sigma(\tau) \approx 1{,}1 \pm 0{,}1 =$ constant, the conversion regime that corresponds to equation (7) is realized at the same level of gas evolution. Increasing T_{exp} causes the shifting of $\eta_{max}(t)$ to the lesser *t*, a decrease in $\Delta\eta = \eta_{max}(t) - \eta_\infty$, and finally a degeneration of $\eta_{max}(t)$: The dependence of η(*t*) becomes a monotonically accelerating relationship (Figure 3.2). The same picture is also observed at the change of the ratio m_0/V (at the constant T_{exp}). Thus, decreasing of the m_0/V ratio results in both a decrease of the value of $\eta_{max}(t)$ in the line of smaller time of conversion due to a decrease of τ (Figure 3.3, curves 1 and 2) and in the disappearance of η_{max} at higher T_{exp} (Figure 3.3, curves 3 and 4). A decrease of $\alpha_\Sigma(\tau)$ is also observed. It should be noted that the similar adsorption of evolved gaseous products during the conversion has been observed earlier during the investigation of thermal transformation of nickel formate [33] and other compounds [34].

For comparison of the thermal stability of the compounds being studied, it is convenient to consider the initial rates of gas evolution: $W_0 = \xi_0 k_1 (1 + \xi_0)^{-2}$. In the range of 573–633 K the metallopolymer being studied can be placed into a series PAA–Ni^{2+} < NiPAcr in which their stability is increased. Figure 3.4 illustrates the yield of the gaseous products during thermolysis of NiPAcr. In an earlier stage of the conversion, the rate of gas evolution is quite high. CO_2 is essentially a single product. The major amount of the product is evolved and then the rate of conversion becomes appreciably lower (Figure 3.4, curve 2). Only when $\alpha_{\Sigma,t} \approx 0.8$ do CO, H_2, and CH_4 appear. The character of their accumulation is different. If the yield of H_2 and CH_4 is monotonically increased with

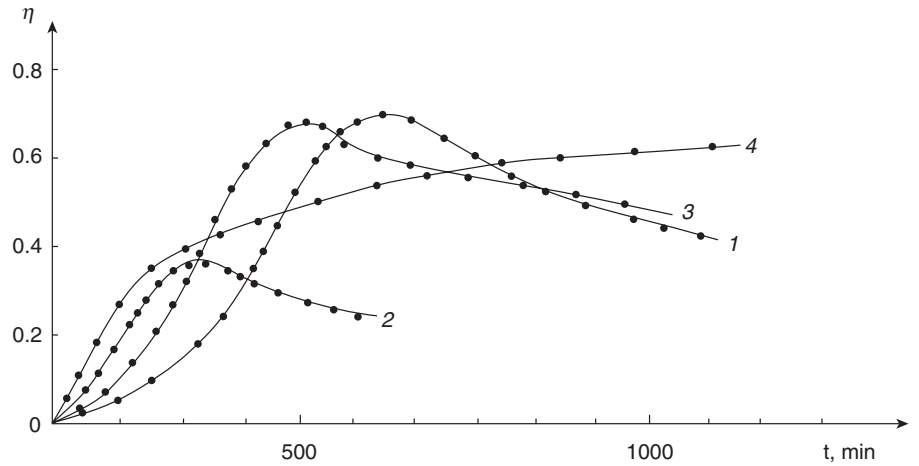

Figure 3.3. The effect of $(m_0/V) \times 10^3$ on the $\eta(t)$ dependence during the NiPAcr conversion: 1, $(m_0/V) \times 10^3 = 2.09\,g \cdot cm^3$, $T_{exp} = 573\,K$; 2, $1.46\,g \cdot cm^3$, 573 K; 3, $2.09\,g \cdot cm^3$, $T_{exp} = 583\,K$; 4, $1.46\,g \cdot cm^3$, 583 K.

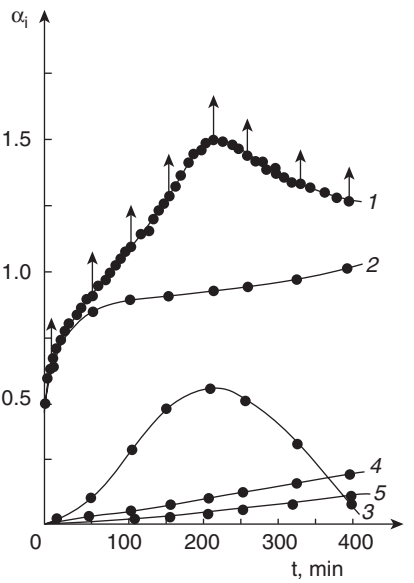

Figure 3.4. The dependence of yield of gaseous products on time during thermolysis of NiPAcr (573 K): 1, $\alpha_{\Sigma,t}$; 2, $\alpha_{CO_2,t}$; 3, $\alpha_{CO,t}$; 4, $\alpha_{CH_4,t}$; 5, $\alpha_{H_2,t}$. The arrow indicates the points of sampling for mass-spectrometry analysis.

the time of conversion, the accumulation of CO passes through a maximum and then falls to the low values (Figure 3.4, curve 3). With T_{ex} the maximum of CO_2 evolution is shifted to the small time range and at $T_{ex} > 583\,K$ is degenerated, as is observed for $\eta(t)$. It is essential that with the falling of the CO yield, some increasing of the rate of CO_2 evolution takes place. Thus, the falling of the total gas evolution in the end of thermolysis of NiPAcr is most probably caused by a consumption of CO at the end of conversion.

The data of IR studies in the example of NiPacr and $Ni(acr)_2$ allowed us to observe the order degree of macromolecular structure during thermolysis by monitoring the character of an appearance and disappearance of the band of regularity (BR) [35]. The bands of regularity are the adsorption bands of the longitudinal vibrations of the lengthy regular parts of a polymer chain. Their intensity is monotonically increased with an increase of a chain length.[2] In the case of NiPAcr, δ_{C-H} at $836\,cm^{-1}$ can belong to BR and ν_{C-H} at $2935 \pm 5\,cm^{-1}$ can be used as the inner standard. Then the $\Psi = D_{836}/D_{2935}$ ratio will characterize the average (the intermediate value between the number-average and number-weight ones [35]) length of the regular part of the polymer chain. For the initial NiPAcr we obtain $\Psi = 0.66$, which can correspond to the average length of the regular part containing 6–10 units. Thermolysis of NiPAcr ($T_{exp} = 573\,K$) at the loss of mass $\Delta m/m_0 = 0.11$ results in the increasing of Ψ to 0.77, but already at $\Delta m/m_0 \approx 0.28$ the BR has disappeared ($\Psi = 0$), which indicates the destruction of the regular structure in NiPAcr.

The solid products of the thermolysis of PAA–Ni^{2+} and NiPAcr (Table 3.2) are the mixture of two phases in the partially X-ray-amorphous matrix. One of them is a well-crystallized phase of metallic Ni, and another is the particularly crystallized phases of nickel oxide (for NiPAcr) and nickel carbide (for PAA–Ni^{2+}). For all the polymers, decarboxylation of metal-containing groups is a source of the largest portion of the total gaseous products. The major product is CO_2:

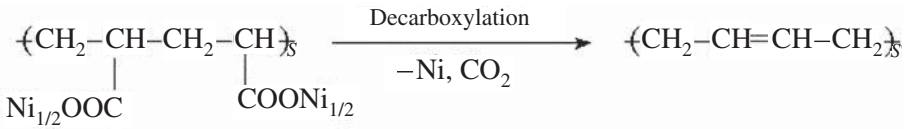

Scheme 3.3.

[2] In the IR spectra of carbon-chain polymers the BR are the bands of C–H deformation vibrations δ_{C-H} (720–950 cm^{-1}) of the backbone, and the bands of stretching vibrations ν_{C-H} (2800–3000 cm^{-1}) are least sensible to the structure of polymer and can be used as an inner standard.

TABLE 3.2. The Composition of Solid-Phase Products of Thermal Decomposition of Ni-Containing Precursors ($T_{exp} \approx 643$ K)

Compounds	Composition
$NiAcr_2$	Ni (~43 wt. %), NiO (~wt. 35%), Ni_3C (~22 wt. %)
NiPAcr	Ni (~wt. 75%), NiO (~25 wt. %)[a]
PAA-Ni^{2+}	Ni(~84 wt. %), NiC[a](~16 wt. %)
Fe_2NiAcr_9	Ni,[b] NiO,[b] Ni_3C[b]
$Ni(Prop)_2$	Ni,[b] NiO,[b] Ni_3C[a]

[a] Partially crystalized phase.
[b] X-ray amorphous phase.

TABLE 3.3. The Yield of Gaseous Products at the End of Thermolysis of Ni-Containing Precursors with Temperature

Compounds	T_{exp} (K)	$\alpha_{\Sigma,f}$	α_{CO_2}	α_{CH_4}	α_{H_2}	α_{CO}
NiAcr	573–643	0.62–2.05	0.55–1.62	0.04–0.38	0.04–0.01	~0.01
NiPacr	563–598	0.98–1.8	0.72–1.50	0.11–0.23	0.10–0.01	0.07–0.14
PAA–Ni^{2+}	573–643	2.06–3.25	1.88–2.74	0.07–0.40	0.09–0.04	0.02–0.07
Fe_2NiAcr_9	603–643	3.34–3.72	2.45–2.52	0.11–0.25	0.75–0.53	0.45–0.60
$Ni(Prop)_2$	603–643	0.87–1.38	0.63–1.02 (0.16–0.30)[a]	0.02–0.04	0.04–0.01	≤0.01

[a] $\alpha_{C_2H_4}$.

H_2 is likely to appear during the course of a catalytic dehydrogenation of decarboxylated polymer matrix under the influence of the Ni nanoparticles formed. However, the contribution of such a process in the total balance of gas evolution is obviously quite small; this is also confirmed by the low values of α_{H2} (Table 3.3).

CO can be formed in the oxidation of metallic Ni formed:

$$Ni_{(s)} + CO_{2(g)} = NiO_{(s)} + CO_{(g)} - 38.5\ \text{kJ/mol} \tag{8}$$

A decrease in the CO yield in the range of high degree of gas evolution is apparently caused by its consumption in the Ni carbide formation:

$$3Ni_{(s)} + 2CO_{(g)} = Ni_3C_{(s)} + CO_{2(gr)} + \sim 122\ \text{kJ/mol} \tag{9}$$

$$4Ni_{(s)} + CO_{(g)} = Ni_3C_{(g)} + NiO_{2(s)} + \sim 84\ \text{kJ/mol} \tag{10}$$

The appearance of CH_4 in the end stages of thermolysis (Figure 3.4) can be determined by the possibility of its formation using the several routes with the

participation of the Ni_n phase when the Ni particles reach certain sizes. This can be a direct interaction of CO_2 and/or Co with metallic Ni to yield NiO [8]:

$$2Ni_{(s)} + CO_{2(g)} + 2H_{2(g)} = CH_{4(g)} + 2NiO_{(s)} + 170.1\ kJ/mole \quad (11)$$

$$Ni_{(s)} + CO_{(g)} + 2H_{2(g)} = CH_{4(g)} + NiO_{(s)} + 208.6\ kJ/mole \quad (12)$$

Alternatively, it can be their catalytic (Ni_n) hydrogenation by H_2:

$$CO_{2(g)} + 4H_{2(g)} \rightarrow CH_{4(g)} + 2H_2O_{(g)} + 165.1\ kJ/mole \quad (13)$$

$$CO_{(g)} + 3H_{2(g)} \rightarrow CH_{4(g)} + 2H_2O_{(g)} + 206.1\ kJ/mole \quad (14)$$

Another way can consist of a catalytic destruction of decarboxylated matrix as follows:

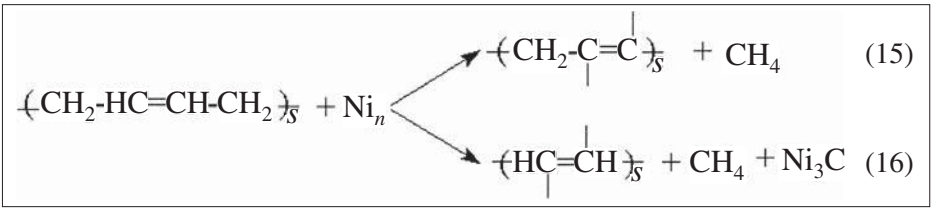

(15)

(16)

The calculations of the composition of solid-phase products with consideration of the balance $\alpha_{Ni} + \alpha_{NiO} + \alpha_{Ni3C} = 1$ and their comparison with data on α_{CH4} have showed that the most probable routes for the formation of CH_4 are the reactions (15) and (16).

Thus, the kinetic peculiarities of solid-phase thermal transformations of metallopolymers is the result of thermal stability of metal carboxylate groups. Their reactivity is determined first of all by a spatial organization of the nearest surroundings—that is, the microstructure of polymer chains. This is confirmed by the presence of bands of regularity, as well as by their appearance on earlier stages of thermolysis followed by their evolution during thermolysis. From the viewpoint of solid-phase topography, metallopolymers are characterized by heterogeneity of the particle reactivity. The qualitative and quantitative composition of gaseous and condensed products essentially depend on the secondary processes with participation of the metal-containing phases formed.

Let us consider the magnetic properties of solid-phase products of the metallopolymer thermolysis. Such products are ferromagnetic. The magnetization of the initial $Ni(Acr)_2$, $\sigma_s(300\,K)$, equals $0.209\,Gs \cdot cm^3 \cdot g^{-1}$; and the specific magnetic susceptibility, $\chi_\sigma(300\,K)$, equals $0.255 \times 10^{-4}\,cm^3 \cdot g^{-1}$. Respectively we estimate the magnetic moment μ_{eff} of 3.40 mB; this value is close to the spin moment $\mu_s = 2.83$ mB, which is characteristic for octahedron symmetry of Ni^{2+}. During thermolysis the σ_s and χ_σ change (Table 3.4).

TABLE 3.4. The Change of Magnetic Properties of the Products During Thermal Transformation of $NiAcr_2$ ($T_{exp} = 643$ K)

$\Delta m/m_0$	σ_s ($Gs \cdot cm^3 \cdot g^{-1}$)		σ_F ($Gs \cdot cm^3 \cdot g^{-1}$)		$\chi_\sigma \times 10^5$ ($cm^3 \cdot g^{-1}$)		η_F	
(wt. %)	300 K	77 K	300 K	77 K	300 K	77 K	300 K	77 K
0	0.209	—	0	—	2.55	—	0	0
19.1	0.235	0.675	0.024	0.041	2.19	6.70	4.4×10^{-4}	7.5×10^{-4}
27.1	0.323	1.447	0.084	0.155	2.53	11.8	1.54×10^{-3}	2.84×10^{-3}
35.4	—	2.177	—	1.240	—	9.9	—	2.28×10^{-2}
46.0	0.93	2.184	0.624	1.949	3.24	11.6	1.14×10^{-2}	1.74×10^{-2}
51.2	14.36	14.95	12.80	13.78	16.7	12/3	0.235	0.235

Notes: $\sigma_s = \sigma(9446\,Oe)$ represents the magnetization in the field of 9446 Oe; $\sigma_F \Rightarrow \sigma(0)$ represents extrapolation of the magnetization to zero field; $\chi_\sigma \cdot = \chi(9446\,Oe)$ represents the specific magnetic susceptibility in the field of 9446 Oe; $\eta_F = \sigma_F/\sigma_s(Ni)$ represents the mass portion of metallic Ni assuming that all ferromagnetism of the sample comes from Ni, σ_s,(Ni) = 54.5 $Gs \cdot cm^3 \cdot g^{-1}$.

The observed nonmonotonic dependence of the σ_s and χ_σ on the time of thermolysis is caused by a drastic increase of ferromagnetic phase formation rate at the end of conversion. At the end of gas evolution, $\eta_F \approx 0.23$–0.25; that is, only 25% of Ni atoms are in a ferromagnetic phase, and the remaining Ni atoms are in a low-magnetic phase. The yield product has the following magnetic characteristics: $\sigma_s(300\,K) = 14.36$ (300 K) and 14.95 (77 K) $Gs \cdot cm^3 \cdot g^{-1}$; $\chi_\sigma \times 10^5 = 16.7$ (300 K) and 12.3 (77 K) $cm^3 \cdot g^{-1}$; $H_c = 8.94$ (300 K) and 53.6 (77 K); $j_r = 0.02$ (300 K) and 0.133 (77 K), where H_c and j_r are the coercive force and the coefficient of rectangle, respectively.

Thus, thermolysis of even relatively simple metallopolymer systems takes place on the multichannel routes, and the properties of the yield products are chiefly determined by the thermolysis conditions.

3. THE PECULIARITIES OF THERMOLYSIS OF METAL-CONTAINING MONOMERS

This perspective method of metal–polymer nanocomposites formation involves the synthesis of both a nanoparticle and its stabilizing polymer matrix in one place (essentially in one stage). Such an approach is conceptually unique, and the systems under consideration are chemically self-regulating ones and thus they have embodied the best solution of the given problem (i.e., the nanoparticles formation and stabilization in polymer systems). Although at present the method is realized on transition metal acrylates and maleinates

only [36], there are no principal limitations for its use with the other types of metallomonomers.

The kinetic studies of the thermal transformations were carried out in the self-generating atmosphere of many simple and clustered acrylates [4–9]: $Co(CH_2{=}CHCOO)_2 \cdot H_2O(CoAcr_2)$, $Ni(CH_2{=}CHCOO)_2 \cdot H_2O(NiAcr_2)$, $Cu_2(CH_2{=}CHCOO)_4(CuAcr_2)$, $Fe_3O(OH)(CH_2{=}CHCOO)_6 \cdot 3H_2O(FeAcr_3)$, their co-crystallizates $[Fe_3O(OH)(CH_2{=}CHCOO)_6] \cdot [Co(CH_2{=}CHCOO)_2]_{2.4}(FeCoAcr_{10})$ and $[Fe_3O(OH)(CH_2{=}CHCOO)_6] \cdot [Co(CH_2{=}CHCOO)_2]_{1,5} \cdot 3H_2O$ (Fe_2CoAcr_9), $NiAcr_2$ and $FeAcr_3$ co-crystallite with atomic ratio of [Fe] : [Ni] ≈ 2 (Fe_2NiAcr_9), maleinate $Co(OCOCH{=}CHCOO) \cdot 2H_2O$ (CoMal), and acid maleinate $Fe_3O(OH)(OCOCH{=}CHCOOH)_6 \cdot 3H_2O$ $(FeMal_6)$. It should be noted that the IR spectra of Fe_2NiAcr co-crystallite cannot be considered as a superposition of the adsorption spectra of two individual compounds. In particular, for $Ni(Acr)_2$ in the region of 920–1020 cm^{-1}, the shifting of the band from 967 to 973 cm^{-1} is observed. Also a new sharp adsorption band at 1001 cm^{-1} appears. The appearance of new sharp bands in the IR spectra of the Fe_2NiAcr_9 co-crystallite is interpreted as a formation of a co-crystallite with a perfect crystal structure. Some common features of thermal behavior of the monomers being studied can be presented as follows [37–45].

The thermal decomposition is accompanied by a gas evolution and mass loss of the samples. A commonness of the processes lies in the fact that the transformations go through three main macrostages with different temperatures:

1. The initial monomers dehydration (desolvation) at 303–473 K
2. The stage of a solid-state homo- and copolymerization of the dehydrated monomer (at 473–573 K)
3. The produced polymer decarboxylation to a metal-containing phase and oxygen-free polymer matrix at $T_{ex} > 523$ K (for copper acrylate, $T > 453$ K) with an intense gas emission

The gas evolution kinetics (Table 3.5) (with reference to a value $\eta(t)$) for all compounds being studied in a general way can be approximated adequately by the expression

$$\eta(t) = \eta_{1f}[1 - \exp(-k_1\tau)] + (1 - \eta_{1f})[1 - \exp(-k_2\tau)] \qquad (17)$$

where k_1 and k_2 are effective rate constants; $\eta_{1f} = \eta(t)$ at $k_2 t \to 0$ and $k_1 t \to \infty$; $\tau = t - t_{\Pi}$; t_{Π} is the sample warming-up time.

Thermolysis of the low-molecular-weight analogue $Ni(Prop)_2$ follows the law of first-order reaction:

$$\eta(t) = 1 - e^{-k1t}(1) \qquad (18)$$

TABLE 3.5. Thermolysis Kinetic Parameters of Transition Metal Unsaturated Carboxylates

			$\eta_{1f}, \Delta\alpha_{\Sigma,f} = A\exp[-\Delta H/(RT)]$			$k = A\exp[-E_a/(RT)]$	
MR_n	T_{ex} (K)	η_{1f}, $\Delta\alpha_{\Sigma,f}$	A	ΔH (kJ/mole)	k	A	E_a (kJ/mole)
$CuAcr_2$	463–513	η_{1f}	1.8×10^4	48.1	k_1	9.5×10^{11}	154.7
		$\Delta\alpha_{\Sigma,f}$	3.6	12.5	k_2	9.2×10^{11}	163.0
$CoAcr_2$	623–663	η_{1f}	1.0	0	k_1	3.0×10^{14}	238.3
		$\Delta\alpha_{\Sigma,f}$	1.55	0	k_2	0	0
	473–573	η_{1f}	1.0	0	k_1	4.2×10^{21}	246.6
$FeAcr_3$		$\Delta\alpha_{\Sigma,f}$	1.6×10^2	25.5	k_2	0	0
	573–643	η_{1f}	1.0	0	k_1	1.3×10^6	127.5
		$\Delta\alpha_{\Sigma,f}$	1.7×10^2	26.3	k_2	0	0
$NiAcr_2$	573–633	η_{1f}	2.6	1.1	k_1	1.7×10^{17}	242.4
		$\Delta\alpha_{\Sigma,f}$	1.4×10^{11}	125.4 (<613 K)			
		$\Delta\alpha_{\Sigma,f}$	1.2	10.5 (>613 K)	k_2	7.5×10^8	156.8
$FeCoAcr_{10}$	613–663	$\eta_{1f} = 0.45(663\,K) - 0.65(613\,K)$			k_1	2.3×10^{12}	206.9
		$\Delta\alpha_{\Sigma,f}$	5.25×10^2	7.5	k_2	6.0×10^8	137.9
Fe_2CoAcr_9	613–663	$\eta_{1f} = 0.35(663\,K) - 0.50(613\,K)$			k_1	2.6×10^{12}	204.8
		$\Delta\alpha_{\Sigma,f}$	1.9×10^2	6.0	k_2	6.6×10^5	125.4
CoMal	613–643	η_{1f}	1.0	0	k_1	1.6×10^6	125.4
		$\Delta\alpha_{\Sigma,f}$	1.3×10^2	23.4	k_2	0	0
$FeMal_6$	573–643	η_{1f}	0.59×10^2	23.4	k_1	3.3×10^7	133.8
		$\Delta\alpha_{\Sigma,f} = 4.78(573\,K) - 7.40(643\,K)$			k_2	1.0×10^7	110.8

and the monomer precursors $Ni(acr)_2$ and $Fe_2Ni(Acr)_9$ decompose according to the equation of the first-order rate of two parallel reactions:

$$\eta(t) = \eta_\infty\left(1 - e^{-k1t}\right) + (1 - \eta_\infty)\left(1 - e^{-k2t}\right) \tag{19}$$

It is interesting that the kinetics of thermolysis for the $Fe_2Co(Acr)_9$ co-crystallite is also approximated by equation (7). The effective energy of activation for the reaction rate k_1 and k_2 are higher (204.8 and 125.4 kJ/mole) than that for $Fe_2Ni(acr)_9$ (129.6 and 79.4 kJ/mole, respectively). The same is true for the values of the preexponential factors (2.6×10^{12} and $6.6 \times 10^5\,sec^{-1}$). At the same time, the values of k_1 for $Fe_2Ni(Acr)_9$ and k_2 for Fe_2CoAcr_9 are close to each other (Table 3.5).

The studied $MAcr_n$ compounds can be ordered according to their transformation initial rates (i.e., by gas emission ability decrease) in the following manner: Cu ≥ Fe > Co > Ni.

The analysis of the gaseous products thermal transformation and the solid product composition (decarboxylated polymer, including metal or its oxide) allows us to determine a general scheme of the metal acrylate thermal transformations:

Initiation

$$\underset{(HR)}{M(CH_2{=}CHCOO)_n} \longrightarrow M(CH_2{=}CHCOO)_{n-1} + \underset{(R'^{\bullet})}{CH_2{=}CHCOO^{\bullet}}$$

$$CH_2{=}CHCOO^{\bullet} + HR \longrightarrow CH_2{=}CHCOOH + (^{\bullet}CH{=}CHCOO)M(OOCCH{=}CH_2)_{n-1}$$

Polymerization

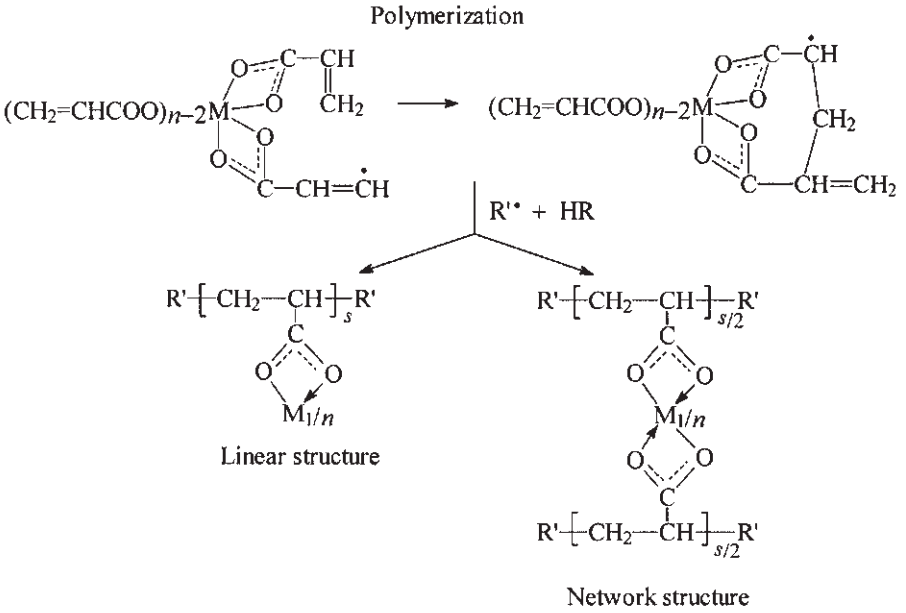

Decarboxylation

$$R'\text{–}[\text{–}CH_2\text{–}\underset{\underset{M_{1/n}(O)C}{|}}{CH}\text{–}CH_2\text{–}\underset{\underset{C(O)M_{1/n}}{|}}{CH}\text{–}]_{s/2}R' \longrightarrow R''[\text{–}CH_2\text{–}CH{=}CH\text{–}CH_2\text{–}]_{s/2}R''$$

$$+ \; xCO + (2s + 2 - s)CO_2 + (s + 2)MO_x$$

R" represents $\dot{C}H{=}CH{-}CH{=}\dot{C}H$ (hydrogen depletion decarboxylated fragment)

MO_x represents a metal ($x = 0$) or its oxide ($x > 0$)

Scheme 3.4.

One of the main transformations is an origin of acrylic CH_2=CHCOO radical in the primary decomposition act that initiates a metal-containing monomer polymerization with a subsequent decarboxylation of metal-containing units. The process temperature has a pronounced effect on the products' yield and their composition. Using EXAFS data [41, 46], it was shown that even at the dehydration stage the metal ligand's surroundings become changed, and during the process such reconstruction is growing. At high temperatures the decarboxylation is accompanied by virtually complete removal of the oxygen-containing units from the polymer matrix.

The studies of nanocomposites' specific surface and its topography [47–49] (Table 3.6) show that they are powders without crystallinity at the distances correlating with transmitted light wavelength. The produced samples have a high value of specific surface (15–30 $m^2 g^{-1}$) and a corresponding dispersity. The mean size of the metal-containing particles (using data on S_{sp}^{f} and assuming the complete polymer decarboxylation) is ~20–30 nm. In some special cases ($CuAcr_2$, $CoAcr_2$, and partially $NiAcr_2$) a dispersion of the big aggregates is observed that results in a decrease of particles mean size and a growth of S_{sp}. At deep stages of the metal carboxylate pyrolysis, the small (<1 μm) opaque particles are observed. Sometimes the fractal-type chain structures of 50–70 μm in length consisting of the agglomerates from the 6–7 primary particles are generated. At the $Ni(Acr)_2$ (T_{exp} = 593 K), thermolysis on earlier stages of conversion the BR with Ψ = 1.27 (δ_{C-H} 830 cm^{-1}, ν_{C-H} 2930 cm^{-1}) appeared which disappeared with conversion and were not observed at T_{exp} – 573 K. The appearance of the BR also indicates that polymerization precedes the major gas evolution. The yield product of thermolysis of Fe_2NiAcr_9 is quite X-ray amorphous.

TABLE 3.6. Dispersity of Starting Metal Carboxylate Samples and the Thermolysis Products

Sample	$S_{0,sp}$ (m^2/g)	$S_{f,sp}$ (m^2/g)	$L_{OM,av}$ (μm)
$CuAcr_2$	14.7	48.0 (463 K)–53.8 (473 K)–43.8 (503 K)	5–50
$CoAcr_2$	20.2	24.1 (623 K)–42.1 (663 K)	100–150
$FeAcr_6$	15.0	15.0	1–5
$NiAcr_2$	16.0	55.0–60.5	60–100
$FeCoAcr_{10}$	9.0	13.6	5–10
Fe_2CoAcr_9	8.1	11.3	10–15
Fe_2NiAcr_9	8.5	13.5	100–200
CoMal	30.0	30.0	5–70
$FeMal_6$	24.0	26.0	30–50

In the case of $Ni(Prop)_2$ a partially crystallized phase (this means that X-ray diffraction spectra has a set of most intensive peaks characteristic for the given phase) of nickel carbide, Ni_3C, is observed. As follows from the X-ray diffraction data, the product of $Ni(Acr)_2$ thermolysis is a mixture of three well-crystallized phases Ni–NiO–Ni_3C with the ratio of $Ni : NiO : Ni_3C \approx 0.51 : 0.81 : 1.0$ [Ni, a face-centered cubic, $a = 0.3524 \pm 0.002$ nm (0.3538 nm); NiO, a face-centered cubic, $a = 0.420 \pm 0.02$ nm (0.4177 nm); Ni_3C, $a = 0.265$ nm, $c = 0.433$ nm (in the parentheses the reference data are given).] Decreasing the T_{exp} to 613 K leads to an amorphization of the product. According to the X-ray data, the particle sizes are ~6.0 nm (Ni, NiO) and ~13.0 nm (Ni_3C); that is, the highly dispersed metal-containing phases are formed.

The topography and composition of the solid-phase products were studied using the electron microscopy and electron diffraction methods, and the results show a morphologically similar picture. There are the electron-dense metal-containing particles of oxides with a near-spheric form. They are presented as the individual particles and aggregates (3–10 particles), and they are uniformly distributed through the matrix space with a lower electronic density. The particles have a narrow size distribution with mean diameter $\bar{d} = 4.0$–9.0 nm (Figure 3.5), and the distance between them in matrix is 8.0–10.0 nm. At the same time, there are some big aggregates in the form of cubic crystals 10.0–20.0 nm in size. The uniformity of the metal-containing particles' space distribution and the narrow size distribution suggest that the decarboxylation and new phase formation processes are largely homogeneous. The estimates show [9] that the mean distance between forming nanoparticle centers is in the range of 7.5–13.5 nm—that is, near the above-mentioned value of 8.0–10.0 nm.

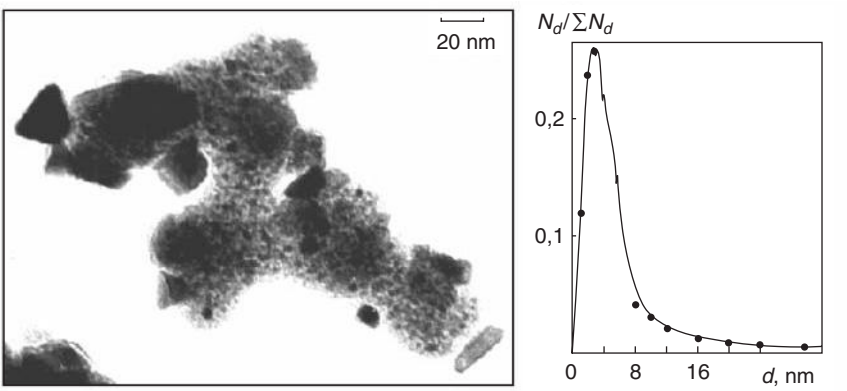

Figure 3.5. Transmission electron micrographs of the product of thermolysis of $Co(OOCCH{=}CHCOO)_2H_2O$ (623 K) and the particle's size distribution.

In the range of 573–633 K the compounds under study can be placed in a series in which their stability is increased: $Ni(Prop)_2 < PAA\text{-}Ni^{2+} < Ni(acr)_2 \leq Fe_2Ni(acr)_9 \leq NiPacr$.

It should be noted that the complication of the spatial organization of metal carboxylated groups leads to an enhancement of their thermal stability. The increasing of the portion of metal carboxylated groups in a polymer chain reveals the same effect. It was found that the end and intrachain metal carboxylic groups of metallopolymer and copolymer formed during thermal transformations also differ in their thermal stability.

In such a manner in the system of transition metal unsaturated carboxylates the nanoparticles synthesis was combined with their synchronous stabilization by the forming decarboxylated matrix [47, 48]. It is safe to assume that further investigations of metal-containing precursor thermolysis in high-molecular-weight media will extend our notions of the interactions and processes in the metal–matrix systems.

Thus, thermolysis of salts of unsaturated mono- and dicarboxylic acid and their polymers usually results in the formation of metal oxides in polymer matrix. At the same time, there exist systems where only metal nanoparticles are formed upon decomposition of some salts. For example, the salts of *m*-carborandicarboxylic acid decompose (at 500–650 K, 2–4 hr) as follows [50]:

$$\left[-OCB_{10}H_{10}CCO-M^{2+} \right]_n \xrightarrow{nH_2O} [C_3B_{10}H_8O]_n + M + H_2OCO_2 + H_2$$

M^{2+} = Mg, Ca, Mn, Cu, Zn, Cd, Ba, Pb

Scheme 3.5.

This is connected with reduction properties of the salts of *m*-carborandicarboxylic acid when, upon heating, hydrogen is evolved [51]. Carrying out this reaction in polymers (for example, polyiminoimides, phenol-formaldehyde resins, etc.) yields the materials containing metal nanoparticles (5–30 nm, depending on temperature) and nonvolatile boron-containing derivatives.

4. THE FORMATION OF METAL SOLS IN POLYMERS BY THERMAL DECOMPOSITION OF THEIR CARBONYLS

Such reactions in the presence of polymers are the most used way to obtain the polymer compositions having a great fraction (up to 90% in mass) of the col-

loidal metal particles. Moreover, at present it is the main method to produce the ferromagnetic nanoparticles being incorporated into polymers due to a macromolecule chemisorption on the nanoparticles directly at their formation moment (*in situ*) including the processes without solvents.

The metal carbonyls are thermolyzed according to the following scheme:

$$Fe(CO)_5 \rightarrow Fe_2(CO)_9 \rightarrow Fe_3(CO)_{12} \rightarrow Fe_n^0$$

Scheme 3.6.

The mechanism of this process includes a chain ion–radical clusterization which in the case of iron carbonyl (it is also close to a decomposition of the IV–VIII group metal carbonyls) can be represented as follows [52]:

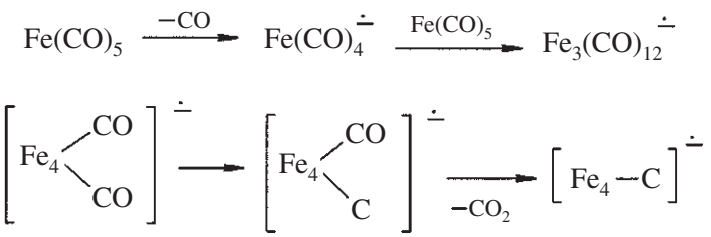

Scheme 3.7.

Under special conditions the metal carbonyls decomposition can be accompanied by formation of not only the metals but also their compounds. For example, one can obtain not only the α-ferrum but also Fe_3O_4 and FeOOH particles and ferric carbides using the following reactions:

$$Fe + CO \longrightarrow Fe_3O_4 + Fe_3C$$
$$Fe_3O_4 + CO \longrightarrow Fe_3C + CO_2$$
$$CO \longrightarrow 0.5CO_2 + 0.5CO$$

Scheme 3.8.

It was shown in [53, 54] that there are two methods to fabricate the homogeneous polymer-immobilized dispersions of colloidal metal particles (Fe, Co, Cr, Mo, W, Mn, Re, Ni, Pd, Pt, Ru, Rh, Os, Ir) using the precursors thermal decomposition. In the former case an "active" polymer solution (containing amino-, amido-, imino-, nitrilo-, hydroxy-, and other functional groups) is used. In an inert solvent a labile metal compound is gradually added to the solution (this operation creates the favorable conditions for the chemisorption interaction) followed by the suspension thermal decomposition at 370–440 K or by radiation.

In the second method a "passive" polymer is used that can react with an initial metal complex after only one ligand is lost (in our systems it is the CO group). Such polymers [e.g., PS (polystyrene), PB (polybutadiene), styrene–butadiene copolymers, etc.] being gradually added to the solution of the inert solvent of the initial complex at the proper temperature leads to the ligand separation, an anion complex bounding with the passive polymer followed by its thermal decomposition.

Some stages of this multistep process (especially the particle growth) are similar to the mechanism of the metal vapor condensation on the polymer [1]. The thermolysis in the presence of polymers was in greater extent studied for carbonyls of cobalt (see, for example, references 56 and 57) and iron [53, 56–58] (Table 3.7) when the process proceeds by a direct $M_a(CO)_b$ vaporization over polymers or by a preliminary adsorption on them.

Particularly the $Fe(CO)_5$ thermolysis in a xylol solution (*cis*-PB or styrene–butadiene copolymer at 408 K, 24 hr, Ar atmosphere) has gone through the successive stages and led to the formation gave rise to the ferrum tricarbonyl(diene) chains $[C_8H_{12}Fe(CO)_3]_n$:

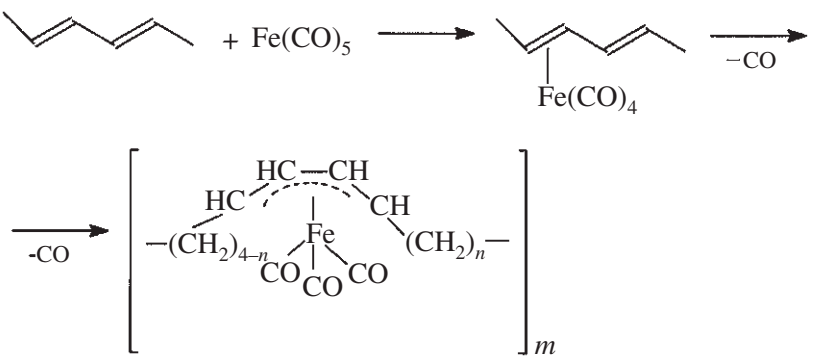

Scheme 3.9.

TABLE 3.7. The Thermal Decomposition of Metal Carbonyls in Polymer Matrices

$M_a(CO)_b$	Polymer Matrix	Thermolysis Conditions	Polymer content in mass (%) and weight and the polymer-immobilized NPs size (in nm)	References
$Co_2(CO)_8$	(Without polymer)	Toluene	>100	55
$Co_2(CO)_8$	PP(atactic)	Toluene	75%; >100	55
$Co_2(CO)_8$	PS	Toluene	75%; 10–30	55
$Co_2(CO)_8$	Polyurethane	Toluene	75%; 5–30	55
$Co_2(CO)_8$	Polychloroprene	Toluene	93%; 30–60	55
$Co_2(CO)_8$	Polyesters	Toluene	75%; 6–20	
$Co_2(CO)_8$	Terpolymer MMA–ethylmethacrylate—vinylpyrrolidone (33 : 66 : 1)	Toluene	20–30	25
$Co_2(CO)_8$	Copolymer vinylchloride–vinylacetate spirit (91 : 6 : 3)	Benzene chloride	75%; 7–47	55
$Co_2(CO)_8$	Copolymer MMA–vinylpyrrolidone (90 : 10)	Benzene chloride	75; 6–25	55
$Co_2(CO)_8$	Styrene–acrylonitrile copolymer (88 : 12)	Toluene	75%; 6–13	59
$Fe(CO)_5$	PB	Decalin, 413–433 K	5–15	53
$Fe(CO)_5$	PB	Decalin, 423 K	~6	58
$Fe(CO)_5$	*Cys*-PB	Xylol, 408 K		57, 58
$Fe(CO)_5$	*Cys*-PB	1% solution dioxane–xylol, 408 K	37% Fe	55
$Fe(CO)_5$	PTFE	DMFA, 413 K	5–15	58
$Fe(CO)_5$	Natural rubber	8% solution dioxane–xylol, 398 K	17% Fe	57
$Fe(CO)_5$	Polystyrene-block-polybutadiene	Dichlorobenzene, 418 K	7–8	53
$Fe(CO)_5$	Styrene–butadiene copolymer (5.8 : 1)	Decalin, 423 K	~6	60
$Fe(CO)_5$	Styrene-4–vinylpyridine copolymer (1 : 0.05)	*o*-Dichlorobenzene	2% Fe; ~6	61

TABLE 3.7. Continued

$M_a(CO)_b$	Polymer Matrix	Thermolysis Conditions	Polymer content in mass (%) and weight and the polymer-immobilized NPs size (in nm)	References
$Fe(CO)_5$	Styrene-4–vinylpyridine (1 : 0.1)	*o*-Dichlorobenzene	1.8 Fe; 16	60
$Fe_3(CO)_{12}$	*Trans*-PB	Benzene, 10% ethanol, 353 K	23% Fe	54
$Fe_3(CO)_{12}$	Styrene–butadiene copolymer (25 : 75)	Benzene, 10% ethanol, 353 K	8% Fe	62
$Fe_3(CO)_{12}$	PB (81% 1,2-chains)	Benzene-dimethoxyethane and 353 K	16% Fe	53
$Fe(CO)_5$	Isotactic PP (melt)		5% Fe	63–65
$Fe(CO)_5$	Atactic PP (melt)		5–30% Fe	63–65
$Fe(CO)_5$	PE (melt)		1–29% Fe; 1.5–7	63–65
$Cr(CO)_6$	PTFE (fluoroplast-40) (melt)		0.5–4% Cr; 1–5	63–65

At the thermolysis initial stage a very active $Fe(CO)_4^-$ anion is formed by reacting with the isolated double bonds, after which the chain double-bond isomerization proceeds generating π complexes with the ferrotricarbonyl residues. The product composed from the η^4-(butadienyl)ferrotricarbonyl chains with trans–trans and cis–trans units. The ferrotricarbonyl complexes having two double nonconjugated bonds are nonstable, and the intermolecular products in such a situation can be formed. A distinctive feature of the process is that the same type of ferrotricarbonyl complexes connected with allylic fragments were identified [66] at the $Co_2(CO)_8$ or $Fe_3(CO)_{12}$ interactions with polystyrene-polydiene block-copolymers. For polystyrene the $M(CO)_3$ fragments connected through the π-complexes with phenyl ring are formed from $M(CO)_6$ (M = Cr, Mo, W) [67].

Such polymer-immobilized π-allylic complexes undergoing thermal decomposition can form nanoparticles in polymer [68], during which the thermolysis can be carried out even without a solvent (for example, by heating of the formed metallopolymer films using an infrared lamp). The nanoparticle sizes depend on many factors such as the characteristics of the used dispersant polymer, its molecular mass (the optimal value is $M_w \approx 100{,}000$), and the nature

of functional groups (L) and solvent. The polymer crystallization proceeds at the solvent removed from the reacting systems, but its supermolecular structure formation depends on the cluster particles concentration and their size distribution. The solvent nature is very important because the $M_a(CO)_b$ complexes in the basic solvents (e.g., in DMF) can disproportionately form the ionic type complexes where a metal formal charge equals +2. The product composition identified by IR spectroscopy depends on the component ratio:

$$n\mathrm{Fe(CO)_5} + 6\mathrm{DMF} \rightarrow \begin{cases} \mathrm{Fe^{2+}(DMF)_6[Fe(CO)_4]^{2-}} + \mathrm{CO} \\ \mathrm{Fe^{2+}(DMF)_6[Fe_2(CO)_1]^{2-}} + 7\mathrm{CO} \\ \mathrm{Fe^{2+}(DMF)_6[Fe_3(CO)_{11}]^{2-}} + 9\mathrm{CO} \\ \mathrm{Fe^{2+}(DMF)_6[Fe_4(CO)_{13}]^{2-}} + 12\mathrm{CO} \end{cases}$$

Scheme 3.10.

In the general case, one has

$$\mathrm{Fe(CO)_5} + \mathrm{Nu} \rightarrow [\mathrm{Fe^{2+}(Nu)_x}]\,[\mathrm{Fe_n(CO)_m}]^{2-}$$

Scheme 3.11.

Here Nu is a nucleophile (Py, *N*-methylpyrrolidone, etc., and $x = 2$–6), $n = 2$ or $m = 8$; $n = 3$, $m = 11$; or $n = 4$, $m = 13$.

The octacarbonyl-dicobalt transformation scheme in these conditions takes the form

$$2\mathrm{Co_2(CO)_8} + 12\mathrm{DMF} \rightarrow 2[\mathrm{Co^{2+}(DMF)_6}][\mathrm{Co(CO)_4^-}]_2 + 8\mathrm{CO}$$

Scheme 3.12.

The basic solvents and high temperatures are favorable to metal carbonyl bonding by polymers and allow us to obtain the stable colloidal dispersions (e.g., with the iron particles 5–10 nm in size) by a carbonyl thermolysis in the dilute polymeric solutions. Such nascent nanoparticles are very reactive; in addition, the small particles (<10 nm) are superparamagnetic and the larger ones (10–20 nm) exhibit a magnetic hysteresis [60].

In solvents with a low dielectric permeability (e.g., in toluene), the obtained Co particles size (2–30 nm with a narrow size distribution) can be controlled by the reaction conditions (temperature, reagents concentration, etc.) or by varying the polymer composition (tercopolymer of methylmethacrylate–ethylacrylate–vinylpyrrolidone [56]).

The nucleophilic fragments of macroligands (particularly in styrene-*N*-vinylpyrrolidone copolymer) bring about a polymer-catalyzed decomposition of the metal carbonyl [53] via the scheme

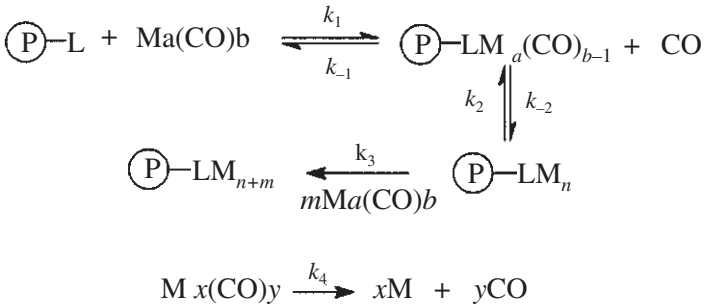

Scheme 3.13.

At the first stage a soluble macromolecular complex is formed with functional groups L. The complex transforms to a polymer-immobilized cluster particle that, after the cleavage of CO groups, undergoes an increase up to a nanoparticle. Actually we see the same development stages as in the above-considered processes of the nanoparticle formation in polymer—that is, the initiation, particle growth, and reaction termination (that can be presented as a simple disproportionation at the particle surface). The main condition for a proper matching of a functionalized polymer is connected with the greater reaction rate on the polymer surface to reduce the decomposition in the solution to a minimum—that is, to provide

$$k_1 + k_2 - k_{-1} - k_{-2} > k_4 \tag{20}$$

$$k_3 > k_4 \tag{21}$$

As a rule, the metal carbonyl decomposition in polar media proceeds by the main reaction routes. First is a main process—that is, the particles growth from the "hot" metal atoms and the formation of nanoparticle having 1–10 nm in size:

$$M_n + M \rightarrow M_{n+1},\ M_n + M_m \rightarrow M_{n+m}$$

Scheme 3.14.

Coincidentally with the forming nanoparticle sizes, a probability of the particles growth termination increases due to their surface noncovalent interactions with macromolecules, although such interactions are weak. First, for the interaction strength on the order of 10^{-4} J/m^2, even the particles of 1–10 nm in size will be captured by macromolecules, and the growth of the particles will be stopped (as a result of an screening effect); that is, the stronger the interaction, the smaller the particle size. For the little and modest-sized particles, the reaction with polymer is described by the following scheme:

$$M_n + \textcircled{P} \longrightarrow \textcircled{P}\text{—}M_n$$

Scheme 3.15.

where (P) is the functionalized polymer.

In effect, it is a chain termination, which usually leads to a nonmagnetic material formation. Second, the disproportionation reaction products interact with the polymer chain, giving rise to some new side reactions (the reticulation, the chain destruction or isomerization, and the mononuclear carbonyl complex immobilization). As, for instance, in 1,4-*cis*-PB (containing 92% of 1,4-*cis*-, 4% 1,4-*trans*-, and 4% 1,2-units with M_w = 246,000) after interacting with $Fe_3(CO)_{12}$ during 2 hr at 350 K, a geometrical isomerization of the chain 1,4-units proceeds and the 1,4-trans units content rises up to 76% [57, 59].

Both of processes run spontaneous, and their competition (connected with the differences of the reacting particles nature and the various reaction conditions) is characterized by a ratio of the thermolysis and the M particles diffusion to the "hot" metal centers in a solid polymer matrix. If the big particles (i.e., big in relation to the distances between the chains, crystalline blocks, or polymer lattice points) are introduced in the system, the polymer structure and its physical and mechanical properties degrade.

In the absence of solvent, the carbonyls thermolysis can be accompanied by some peculiarities. In some systems the Fe, Cr, Co, Ni, and Mn carbonyls can have a catalytic action on the polymer carbonization and graphitization processes—for example, in petroleum, mesogenic pecks (the specific matrices with polycondensed aromatic structures) are able to act as π-ligands stabilizing

the metal clusters [70, 71]. Even the 1% content of metal carbonyl catalyzed the mentioned processes, but the iron content rise up to 5% (at 423 K) leads to noticeable growth of the structures similar to that of graphitic layer compounds.

It can be noticed too that polymers having more polar groups promote the finest particles growth, and the same can be said about the metal carbonyls concentration in polymer. For a thermal $Fe(CO)_5$ decomposition in PEHP matrix a bimodal distribution of the ferrum particles size is observed (with the mean sizes of the distribution modes equal to 2–3 and 4–10 nm) and the particles content is ~20% and 80% (in volume) correspondingly as is shown on Figure 3.6 [72]. The majority of the oxide Fe_3O_4 particles has dimensions ~5 nm.

An original method of metallopolymer production by precursors thermal decomposition is to localize the particles being formed due to a fast monomolecular decay of the solutions containing the metal compounds in polymer melts—that is, in the natural voids of the polymer matrix (as PE, PP, PTFE, etc.). Such materials are called "cluspol" [30, 63–65], and for their production it is necessary to provide the most possible melt temperature, which must be considerably above the temperature of the carbonyl decay initiation. For this purpose the carbonyl dilute solutions are used under these conditions, providing the ultimately fast and complete removal of the split out ligand from the reaction system. Such an approach has many advantages because the temperature rise from one side promotes the metal-forming precursor decomposition and from other side decreases the by-products yield. Furthermore, in a melt (as

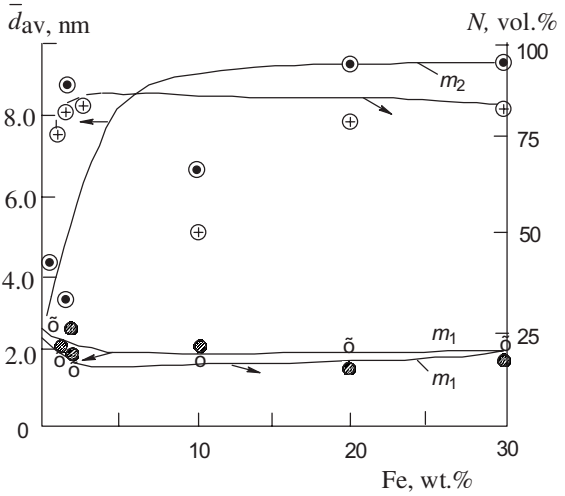

Figure 3.6. The curves of Fe nanoparticles' distribution on the size in a PELD matrix (m_1 and m_2 are the first and second modes of distribution, respectively).

distinct from a solution) a short-range order of the initial polymer structure is preserved, and its voids become readily available for the forming nanoparticles localization.

The obtained polymer-immobilized nanoparticles are characterized by a relatively high dispersion, a uniform distribution through polymer volume, and nonreversible macromolecules sorption on their surface. They are localized primarily in the disordered interspherulite regions of the matrix, between the lamellas or in the spherolite centers. Such a disposition hampers a segmental motion of the amorphous phase for a free volume decrease and a possible interlacing. As a result, the polymer thermostability increases (e.g., the T_m value for atactic PP increases by 50–80°C) and the products represent the monolithic (pseudocrystalline) materials. The spatial periodicity of the ferrum clusters in such structures depends on concentration and averages between 9 and 12 nm for high (20–30% in mass) and 20–22 nm for low (2–3% in mass) concentrations. The particle size distribution is narrow (the half-width is about 1 nm), and it is also possible that the nanoparticles in the matrix intermolecular voids favor the polymer crystalline phase destruction and its transformation to an amorphous state.

It is of interest that neither physical nor chemical properties of such materials allow us to detect a metallic phase for the strong polymer–NP interactions that provide the polycrystalline matter formation. In other words, such products at the same ingredients ratio present the monophase metallopolymers. The nanoparticles' size and distribution depend on the polymer's chemical nature; that is, PEHP, an alternating copolymer of ethylene and carboxide, polyacetonaphthalene, polycarbonate, and so on [72]? With a rise of the nanoparticles' contents in such polymers, naturally their coherent scattering region (CSR) is wider and the crystallinity degrees of PEHP and polycarbonates rise (Table 3.8). At the same time, the polymer matrices cannot preserve the nanoparticles from an oxidation (for example, the ferric nanoparticles in PEHP with the mean size 50 nm after oxidation transforms into Fe_3O_4 particles of the same size).

It is of interest that metal carbonyls such as $Co_2(CO)_8$ form complexes with polyionic ligands (such as ethynylbensene-$Co_2(CO)_6$) and can be decomposed explosively [73] at 513 K (generating CH_4 and H_2) and at 1070 K (forming multilayer nanotubes). It is possible that a metallized polyione pyrolysis can lead to the single-wall nanotube formation too [74], just as the $Fe(CO)_5$ pyrolysis (at 1320 K) in the presence of other carbon sources [75]. The thermal treatment of platinum and cobalt containing poly(phenylene diacetylenes) leads to the Pt (1–3 nm) or Co (5–100 nm) cluster formation into the carboglasses [76].

Another way of the metallocomposite production by the precursor thermolysis is the metal carbonyl decomposition in the halide-containing matrices. Using the above-mentioned classification, such methods can be related to the "passive" ones. The PETF modifications can be performed by Fe^{3+} or Mn^{4+}

TABLE 3.8. X-ray Diffraction Characteristics of Fe-composites Materials

Composite	CSR (nm)	Crystalline Phase Content (%)	Nanoparticle
An alternating copolymer of ethylene and carboxide	20	—	—
+10% Fe	21	—	—
+30% Fe	23	—	—
+50% Fe	23	—	α-Fe, 16.5 nm Fe_3O_4, 5 nm
Polyacenaphthylene	2.5	—	—
+0.1% Fe	2.6	—	—
+1% Fe	2.6	—	—
+10% Fe	2.6	—	Fe_3O_4, 3.5 nm
Polycarbonate	8.0	65	—
+0.5% Fe	9.0	60	—
+1.0% Fe	9.0	60	—
+5.0% Fe	10.0	50	—
+10% Fe	10.0	40	—
PEHP	21.5	30	—
+1.0% Fe	21.5	30	—
+5.0% Fe	26.5	20	—
+10% Fe	25.0	15	Fe_3O_4, 5.5 nm

oxides [77–79] using the sorption of the proper carbonyls and their subsequent decomposition under the action of $KMnO_4$ or H_2O_2. After these reactions the oxides are introduced into the amorphous regions of PETF. The most common situation is that nanoparticles, derived in a polar solvent, are forming the complicated complexes with metal carbonyls that are able to react with fluoropolymers. The main factors affecting a selective interaction of $Fe(CO)_5$ or $CO_2(CO)_8$ with PETF during the thermolysis are generalized in references 80–82. The IR-spectral method allows us to fix the cation–anion $[Fe(DMF)_6]^{2+}[Fe_3(CO)_{11}]^{2-}$–PETF and $[Co(DMF)_6]^{2+}[Co(CO)_4]^{2-}{}_2$–PETF complex formation during adsorption that allows us to perform the kinetic studies of the process as a whole and perform the thermal decomposition in particular. The intermediates thermolysis (413 K, DMF) is a first-order reaction, but these processes' rate constants and activation energies differ essentially (Table 3.9).

Attention is drawn to the fact that the rate constant of polymer-immobilized cobalt carbonyl is very high (its order of magnitude is compar-

TABLE 3.9. The Characterization of Thermolysis of Metal Carbonyls in PETF Matrix

	PETF–$Fe(CO)_5$	PETF–$Fe_3(CO)_{11}^{2-}$	PETF–$Co(CO)_4^-$
$k \times 10^{-5}$, s^{-1}	8.41	12.2	104
E_a ($kJ\,mole^{-1}$)	142.6	51.62	45.80

able with the value for ferrum carbonyl), which correlates with a higher reactivity of the cobalt carbonyl anion. The very high value of E_a for the neutral $Fe(CO)_5$ decomposition in PETF (as compared with the immobilized compounds) suggests that the reactions have different mechanisms. The Fe and Co carbonyls' thermolysis *in situ* leads to the heterogeneous metal domain formation in a polymeric martix. The polymer-connected carbonyls (both for Co and Fe) generates the systems with uniformly distributed ferromagnetic particles having 5–10 nm in size and mean surface from 80 to 700 nm^2 per particle.

The electron diffraction analysis of such systems [81] have revealed the formation of γ-Fe_2O_3 and FeF_2 particles for initial $Fe(CO)_5$ and revealed Co, Co_2O_3, and CoF_2 for initial $Co_2(CO)_8$. The metal fluoride formation is connected with the reactions involving the polymer chain and is accompanied by the C–F bond splitting:

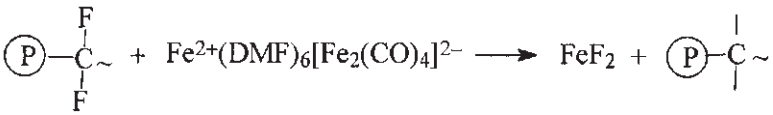

Scheme 3.16.

It follows that in such systems the two processes take place simultaneously. The main process is nanoparticle formation due to a thermolysis, and a side process is an attack of a polymer chain by metal ions whereby the polymer goes through the various transformations (destruction, crosslinking, bounding with the metal complexes, etc.). Moreover, the secondary carbonium ions (formed from PETF) are very active and can be involved in many chemical reactions. As an illustration, atomic zinc interacting with the PETF surface formed ZnF_2 [83, 84]. The characteristics of the bonds between formed clusters and nanoparticles with polymer matrix and their topography are not established conclusively, but it is evident that the polymer–metal particle interactions are defined by the reactivity of metallocenters formed during the decomposition.

It is possible [85] that introducing $Co_2(CO)_8$ into the toluene solution of styrene block-copolymer with 4-VPy also gives rise to the cation–anion complexes localized into a micelle having 4-VPy units (similar to DMF) with com-

position $[Co(4\text{-}VPy)_6]^{2+}$ $[Co(CO)_4]^{2-}$. A topochemistry of such nanoparticles and their sizes or forms are defined by molar ratio [4-VPy]/[Co], because the bounded (in micelles) cobalt after a fast thermolysis at 383 K forms small particles growing at the expense of dissolved $Co_2(CO)_8$ up to the spheroids (~10 nm in size) or the star-like particles (with the nonregular forms and mean sizes 20–23 nm) built up from the initial anisotropic clusters. Only if $Co_2(CO)_8$ is present in large excess do the nanoparticles begin to originate and grow out of the micelle (cubes with mean size 21 nm). As a rule, such particles are vastly larger than the particles formed, as an example, during $CoCl_2$ reduction by superhydride $Li(C_2H_5)_3BH$ [86].

In the last few years there have been new trends in the metal carbonyl decomposition in the presence of polymer namely the sonochemical reactions [81–91] connected with the known effect of the acoustical cavitation, including the bubbles initiation, growth, and explosive "blow-in" into a high-boiling-point solvent. The process is characterized by a high local temperature (several thousand of degrees) and pressure (150–200 MPa), along with the acoustical emission of the excited particles, called *sonoluminescence*. In our problems the acoustic field helped to generate the high-volatility metal compounds (particularly from metal carbonyls) with their subsequent agglomeration in the presence of organic polymer (e.g., PVP [92]) or inorganic (silica gel) polymer up to the polymer-stabilized nanoparticles. The general scheme of such sonochemical synthesis of nanostructured materials can be present as follows:

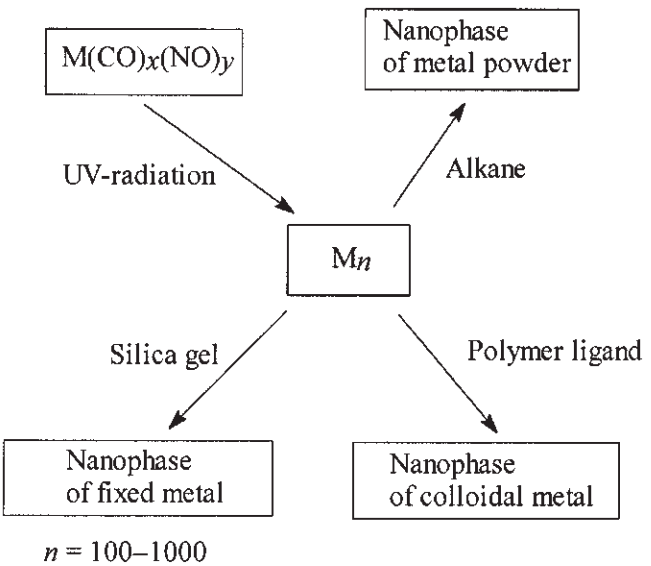

Scheme 3.17.

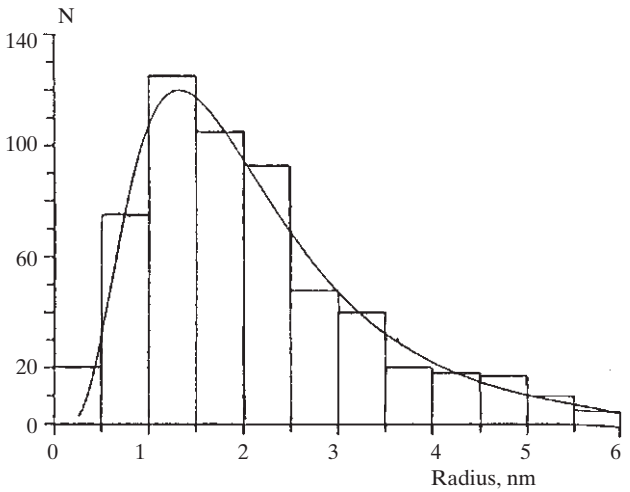

Figure 3.7. The experimental histograms of Fe/PFO nanoparticles' distribution on the size (*N* represents the total number of particles).

Such a reaction of $Fe(CO)_5$ (at 293–363 K, PVP) without ultrasonic radiation proceeds very slowly; and only after few days there, a material is formed with very low Fe content (2%, the isolated particles 2–5 nm in size). It is of interest that the sonochemical decomposition of $Fe(CO)_5$ does not proceed in the presence of PVP if THF is used as the solvent, but the reaction is very effective when anisole is used as the solvent and PFO is used as the polymer matrix [93]. A black product formed contains up to 10% (in mass) of the spheric particles of nonoxidized Fe (mainly γ-Fe, with little content of α-Fe) with 1–12 nm in size (the mean diameter is 3 nm, as shown in Figure 3.7). It is likely that the big particles present the flocks of little ones (~2–2.5 nm). The sonochemical synthesis allows us to produce the functionalized amorphous nanoparticles of ferric oxide with 5–16 nm in diameter [94]. The ultrasonic irradiation in the PFO presence allows us to also produce the stabilized nanoparticles of copper, gold, and so on. In the literature the findings are not about the bimetallic particle formation in the ultrasonic fields by carbonyl metal reduction in the polymer matrices' presence (as, for example, in the case of the carbon-supported Pt–Ru from $PtRu_5C(CO)_{16}$ reduced clusters [95]).

5. POST-THERMOLYSIS OF OTHER-TYPE PRECURSORS IN POLYMER MATRICES

Besides carbonyls, some other metal-forming precursors (usually formiates, acetates, oxalates, or organometallic compounds) are used to produce the

polymer-immobilized nanoparticles by thermolysis. For example, a metal–polymer composition can be prepared by thermolysis of a copper formate triethylene–diaminic complex $[Cu(EDA)_3](HCOO)_2$ into PS through a common solvent (DMF) [96]. The complex decays at 443 K and forms metallic copper in a highly dispersed state. It is of interest that the process temperature in PS is at 20° lower than in a bulk copper formate, which may be associated with a polymer catalytic action on the complex thermal decomposition.

The mechanism of the process is that the polymer reactive centers promote the metal nucleation and aggregation, after which the thermolysis occurs and the metal-containing substance is redistributed. The maximum amount of copper being introduced in PS through a common solvent is about 10%. At the same time, the polymer presence increases the temperature of cadmium trihydrate–oxalate decomposition [97], and the decay products increase the initial temperature of PETF intensive destruction. The copper formate thermal decomposition in the highly dispersed PETF presence allows us to produce a metallopolymeric composition (20–34% of copper) where the NP size distribution is maximal at ~4 nm, without any chemical interaction between the components.

At high temperature thermolysis (1270 K) of cobalt acetate with PS, PAA, and PMVK present, the metal clusters that are catalyzing an oxygen electrolytic reduction had formed [98]. As the thermal decomposition of silver trifluoroacetyl-acetonate at 613 K occurs in polyimide film [99–101], the film becomes metallized (a structure called "film on film") and a nanocomposite is formed with high surface conductivity and light reflection coefficient (above 80%).

There are some examples of the nanoparticle formation in polymers by metal hydroxide decomposition [102]. The thermal decay of silver hydroxide ammonia solution in the isotactic PP melt (temperature range 543–563 K in polymethylsiloxane) occurs according to the following scheme:

$$4[Ag(NH_3)_2]OH \rightarrow 4Ag^0 + 8NH_3 + 2H_2O + O_2$$

Scheme 3.18.

The silver content in PP varies from 3% to 15% (in mass), the particle sizes change in a wide range (2–25 nm), and the small particles (<5 nm in diameter) are roentgen-amorphous but the bigger ones have a crystalline structure.

The Pd particles (with $S_{sp} = 26\,m^2/g$), produced by the decomposition of a palladium hydroxide fine dispersion in PVC, formed the space structures with the nodes where the highly dispersed Pd particles are located [103]. It must be noted that such a structure increases the temperature of PVC complete dehydrochlorination.

An original method of copper-containing composite production on a porous PELP base (obtained by crazing method) is connected with use of a Cu^{2+}–monoethanolamine complex [104]. The complex simultaneously combines the functions of an adsorption active medium, a complex-forming agent, and a copper ion reductant. Under the complex decay (at temperatures from 363 to 398 K), the copper nanoparticles are forming in the porous PE. They have a wide size distribution (from 60 to 320 nm), and the metal mass content is about 8%. It is worthy to note that even a little amount of such filler (1–2 vol. %) improved considerably the polymer mechanical properties. Also, we must note that there is a recently developed universal method for the synthesis of nanocomposites on metal nanoparticles (or their sulphide) embedded in polymer matrices by thermolysis of metal *n*-alkanthiolates $M_x(SC_nH_{2n+1})$, where $n = 12$, 16, and 18 at moderately low temperatures (390–470 K) in a polystyrene matrix [105]. Metal nanoparticles are homogeneously distributed in a polymer matrix and have mean sizes of 7 nm (Pd) and 10 nm (Ag and Au). The size of particles can be controlled by the concentration of the precursors, as well as by the thermolysis time and temperature.

Some examples are of interest from the very limited findings about nanoparticles formation by organometallic compound decomposition in polymers. The cryochemically synthesized bisarene complexes $(C_6H_5CH_3)_2M$ (M = Ni, Co) were subjected to a fast decomposition in PELD at a temperature higher than that of the complex decay. The metal content in material produced achieved 1.4–4.3% [106]. The cobalt nanoparticles (mean size ~1.6 nm, a narrow size distribution) were obtained by H_2 reduction of organometallic precursor $Co(\eta^3\text{-}C_8H_{13})(\eta^4\text{-}C_8H_{12})$ at PVP presence at 273–333 K [107]. As a precursor, bis(cyclooctatetraen)-iron $Fe(C_8H_8)_2$ can be used too [108]. By contrast, the similar ruthenium complex $Ru(\eta^4\text{-}C_8H_{10})(\eta^6\text{-}C_8H_{12})$ had decomposed slowly even at 0.3 MPa in the presence of PVP. The Mo, Cr, and W hexacarbonyls do not photochemically decompose at high pressures (~35 MPa) of N_2 or H_2 and low temperatures (~30 K) in polyethylene matrix but gave the different substituents only [109] as well as ferrum carbonyls in PE matrix at 190 K [110]. The nanoparticles of Ru (~1.2 nm) [111], Pd, and Pt [112, 113] also can be produced from the organometallic precursors in PVP matrix at 298 K. Nickel dicyclo-octadiene $Ni(COD)_2$ can spontaneously decay (at room temperature in PVP dichloromethane solution), forming the particles with mean size 2–3 nm [114]. The nanocomposites can be obtained in the same manner (by precursor decomposition) based on Nafion-type films of ionic polymer [115–117].

An original method of orgametallic compounds impregnation into the PS, PEHP, and PETF amorphous regions and polyacrylates with their subsequent structural modification and clustering is based on the usage of some liquids in a supercritical state (CO_2, 8–25 MPa, 303–313 K), as was shown for cymanthrene $(\eta^5\text{-}C_5H_5)Mn(CO)_3$ [118]. In another method the platinum dimethyl-

cyclooctadiene(II) precursor was dissolved in CO_2 and the thin films of poly(4-methyl-1-pentene) or PETF were impregnated by the solution [119, 120]. After reduction (by thermolysis or hydrogenolysis) the polymeric nanocomposites are formed with Pt particles (15–100 nm in size). The kinetic data of impregnation for manganese cyclopentadienyl-tricarbonyl and copper hexafluoroacetylacetonate, dissolved in the supercritical media (CO_2), show that the process is very intense in the polymer amorphous regions, very weak in the partially crystalline regions, and practically absent in crystalline ones [116].

In summary of this section, it must noted that, in spite of numerous studies, nowdays we know very little about carbonyl hydrides and other substituted (mixed) carbonyls thermolysis in polymeric systems, as well as in reactive plastics. For example, in some experiments the decomposing metal carbonyls were placed into an epoxide resin heated up to the nanoparticles deposition on the forming polymer surface [121]. It is possible that the highly reactive metal particles in such systems can initiate the epoxy cycle cleavages followed by a three-dimensional space structure formation. Iron carbonyl being decomposed into polybenzimidazole suspension (in transformer oil at 473 K) forms the ferrum nanoparticles (1–11 nm) capable of polymer thermostabization [122].

It should be stressed that the considerable simple picture of the nanocomposites formation is observed only when for the thermolysis the thermally unstable substances are used (such as the metal-containing precursors); otherwise the polymer matrix thermal destruction (i.e., the reactions connected with the chemical bond breakage and radicals generation) begins to play an important role along with the nanoparticle formation processes. The thermodestruction products present low-molecular-weight volatile compounds of complex type (including monomer) and nonvolatile residue, subsequently becoming a carbonized structure. On the other hand, the highly dispersed metals of alternating valence or their lowest oxides (Fe, FeO, Ni, Cu, etc.) with a defective structure are often introduced into a polymer, especially to inhibit its thermal or thermooxidative destruction processes [123, 124]. For example, the small amount of iron particles in PEHP (0.05–1.0% in mass) increases its thermal stability in comparison with the pure polymer. Of interest is the method of "non-chain" inhibition of thermal oxidative destruction of thermostable polymers [124] based on oxygen binding with highly effective acceptors—that is, metal nanoparticles formed in polymer matrix (i.e., acceptors for oxygen are formed directly in matrix).

It must be noted that the metal-containing precursors and the nanoparticle interactions with the polymer matrix (formed under the pyrolysis), as well as the product topography, are not sufficiently studied, but it is no question that a role of metal centers and their activities are very important for the general picture of the metal particles' interaction with a polymer matrix.

6. THE COMPUTER MODELING OF ASSEMBLING OF METALLOPOLYMER NANOCOMPOSITES DURING CONTROLLED THERMOLYSIS

As shown above, the synthesis of metallopolymer nanocomposites through solid-phase thermal transformation of both macromolecular metallocomplexes and metal-containing monomers—in particular, transition metal carboxylates of unsaturated acids—is a very promise and perspective way. In such processes the formation of nanoparticles, along with their matrix stabilization, occurs simultaneously and is connected with the self-organization of nanoparticles during thermal transformation. This process results in the formation of composites containing (depending on the nature of the metal-containing groups) metal or metal oxide nanoparticles with a quite narrow distribution of size and is homogeneously located in the volume of stabilized matrix.

Although the solid-phase thermal process combines a set of multistage physicochemical transformations [125, 126], on the whole it can be represented by the following simplified scheme of transformations [127].

Thermal decomposition of metal-containing polymer fragment:

$$ML_r \rightarrow M^* + rL \tag{22}$$

Cluster formation and nanoparticle growth:

$$M \xrightarrow{M} M_2 \xrightarrow{M} M_3 \xrightarrow{M} M_{n-1} \xrightarrow{M} [M_n] \tag{23}$$

Polymerization of demetallized polymer ligand (L_r):

$$rL \rightarrow L_r \tag{24}$$

where M is a metal, M* is a metal atom or metal-containing molecule, and L is an unsaturated ligand.

A current wide set of experimental data concerns mainly the yield characteristics of systems such as nanoparticle distribution in the size and matrix space, physical and chemical properties of the matrix formed, and so on. At the same time, the investigations on the mechanism and kinetics of nanocomposite formation and on understanding how these parameters change during thermal transformations are absent because of the difficulties of the experimental studies of the kinetics of such processes.

Computer modeling is the simplest and most productive approach for studying kinetic processes. In recent years the varied variants for solving these problems have been developed [127, 128]. Thus, in the frame of the model of diffusive-restricted aggregation the computer modeling of the kinetics of

nanoparticle formation in the solid phase during thermolysis of metal-containing macroligands is performed using the Delphi program in Windows [129]. As the basis of the kinetic model, a polymer medium of different structure—isotropic (globular) and anistropic (layer and fibril) ones)—is used. The polymer chains may contain regular or nonregular metal-containing groups. The products of thermal decomposition of reactive metal-containing groups of polymer chain—monoatomic metal particles or its oxide—can be considered as a source of the aggregated particles. The medium in which the transformations (motion and growth of cluster-forming particles) occur were represented as a three-dimensional lattice consisting of $50 \times 50 \times 50$ cubic-cell-reactive groups (1.25×10^5 centers). The size of the cell ($a = 10^{-9}$–10^{-8} m) is varied and is determined by the size of the specific fragment of a regular polymer chain that contains one reactive decaying metal-containing group.

The computer model is based on the following determinant algorithms:

1. Decomposition of metal-containing groups of polymer with formation of monoatomic metal (or its oxide) particles. The rate of the process W_J is described by the law of first-order reaction $W_J = kC = Ck_0\exp[-E_{aJ}/(RT)]$, where C is the current amount of the reaction centers ($C_0 = 1.25 \times 10^5$ monoatomic centers), E_{aJ} k_0, and T are the varying parameters, namely, the energy of activation, preexponential factor, and temperature of thermolysis. Algorithms take also into account the probability of catalytic decay of reaction centers by diffusing particles.
2. The solid-phase diffusion of monoatomic metal (or its oxide) particles to give multiatomic cluster particles. It is assumed that diffusion processes in the solid phase are activated. The rate of diffusion $W_{D,N} = D_N C^* = C^* D_1 \cdot N^{-1/3}$, where $C^* = C/a$ is the current amount of reaction centers per one cell of the a size, N is the size of N-atomic cluster, $D_1 = D_0\exp[-E_{aD}/(RT)]$ is the diffusion coefficient for a monoatomic particle, E_{aD} and $D_0 = \nu\exp(\Delta S/R)$ are the varying parameters, the energy of activation, and the entropy factor ($(\nu \sim 10^{12}\,\text{sec}^{-1})$). Such a model assumes that the coexistence of two or more separate particles in one cell is not possible because they immediately form a single cluster. In the isotropic medium the diffusing particle with a corresponding probability can move in one of the 26 directions.
3. Taking into account the cluster dissociation in the reaction $[M_n] \rightarrow [M_{n-1}] + M$ with formation of multiatomic particles that move to the neighbor cells. The rate of process $W_N = k_N C_N = C_N k_{0N}\exp[-E_{aN}/(RT)]$ depends on the cluster size N and diminishes with its growth, C_N is the current concentration of cluster particles of the N size, and E_{aN} and k_{0N} are the energy of activation for the N-cluster and preexponential factor ($\sim 10^{13}\,\text{sec}^{-1}$), respectively. The energy of activation can vary and

increase from E_{a2} (the energy of activation for two atomic cluster) to $E_{a,\infty}$ (the energy of activation for nanoparticle). $E_{a,\infty} \approx E_{\text{sub}}$ is the energy of sublimation for a bulk metal.

4. Visualization of cluster formation. The algorithm allows us to observe the dynamics of the particle growth and their distribution of size as a function of the initial parameters during the computer experiment. The typical picture of the particle growth scanning is represented in Figure 3.8.

At the end of the experiment the following dependencies are obtained: [$\ln(C + 1)/\ln(C_{\max} + 1)$, t, N] represents the time dependence of cluster distribution on the size, where $C_{\max}$ is the maximum amount of clusters in the moment of time t; [J, N] is an ultimate distribution of clusters on the size where J is the amount of N-size cluster.

The time of iteration, $\Delta\tau$, equals $a^2D^{-1}e^{-2}\xi^{-1}$, where ξ is the varying iteration coefficient ($\xi \geq 1$). The time of experiment, t_Σ, equals Rt_{polym}, where t_{polym}

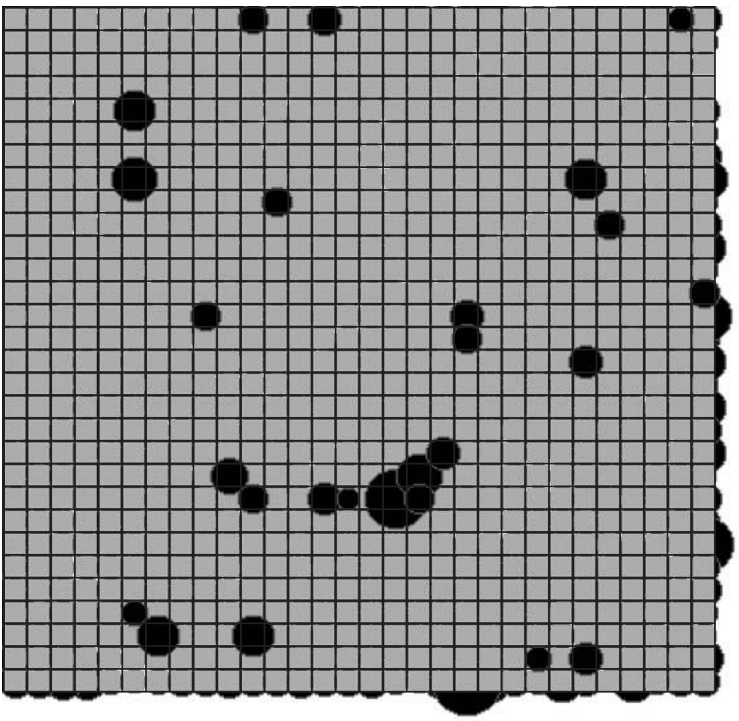

Figure 3.8. A picture fragment of 50 × 50 × 50 cluster growth during the computer experiment.

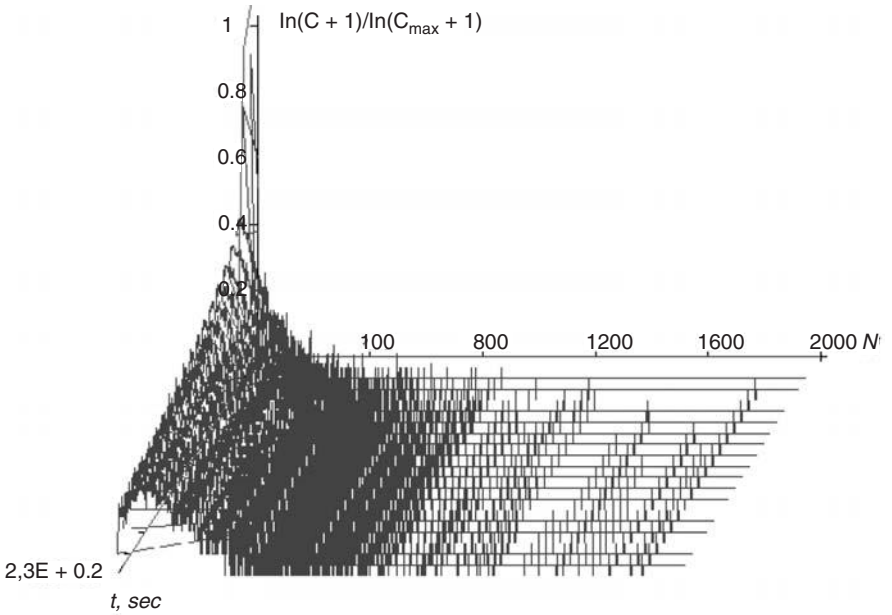

Figure 3.9. The distribution of clusters on the size during the experiment: T = 653 K, $W_{D,N} = 1 \times 10^{-18}$ at·m^2·sec^{-1} (E_{aD} = 250 kJ·mole^{-1}), $W_J = 2.2 \times 10^{25}$ at·m^{-3}·sec^{-1} (E_{aJ} = 167 kJ·mole^{-1}), $W_2 = 1 \times 10^3$ at·m^{-3}·sec^{-1}(E_{a2} = 125 kJ·mole^{-1}), $W_\infty = 4 \times 10^{-14}$ at·m^{-3}·sec^{-1}($E_{a\infty}$ = 330 kJ·mole^{-1}).

$= -k^{-1}\ln(C/C_0)$ is the time of decay of reactive metal-containing groups of polymer ($C/C_0 = 5 \times 10^{-3}$), and R is the relative (varying) time of the cluster formation ($R \geq 1$).

The investigations carried out showed that increasing of cluster formation duration results in the change of spectra of the particle size distribution: With increasing R, the $J(N)$ spectra are shifted into the higher value of N (Figure 3.9). It was found that the conversion is a successive process. For example (Figure 3.10), for the time $t_\Sigma = 228$ sec ($R = 5$) the yield of clusters with $\bar{N} \approx 2$, 37, 65, and 125 passes through maximum, at which the particles with $\bar{N} \approx 65$ have disappeared at $t \approx 200$ sec. It was found that the structure of the polymer medium (layers or fibrils) displayed the considerable effect on the particle size distribution. If the space between the layers or fibrils is inert—that is, outside of the thermolysis zone the nanoparticles are not formed—the size distribution spectra are shifted into a region of lesser sizes (Figure 3.11).

The model considered can be useful for studying the kinetics and mechanism of the formation of metal-containing clusters and nanoparticles in the polymer medium with reactive metal-containing groups. The methodology of

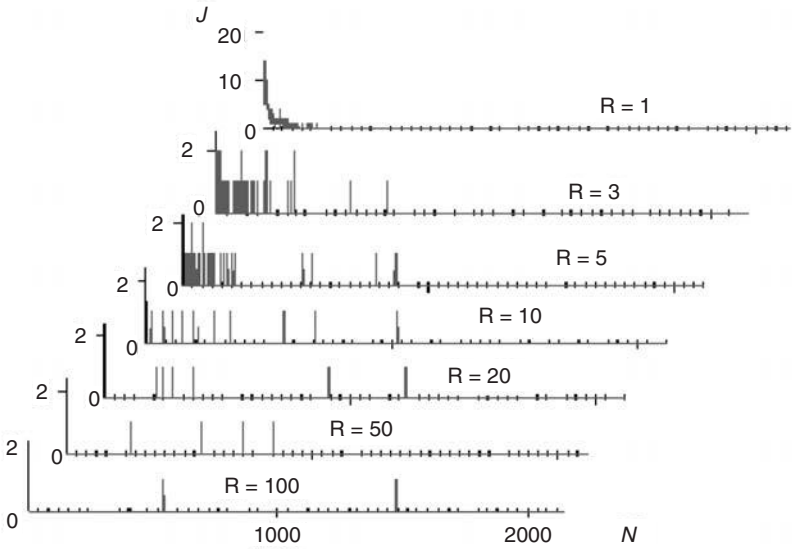

Figure 3.10. The effect of the relative duration of cluster formation on the particle size distribution. Globular structure.

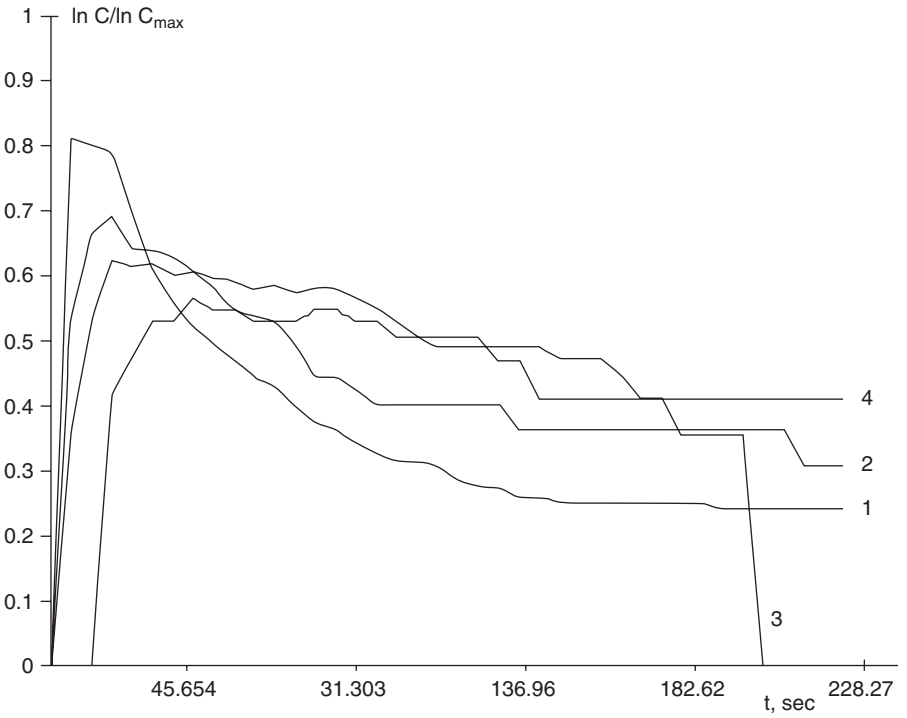

Figure 3.11. The kinetics of the cluster formations. *1*, 1 > *N* > 4; *2*, 35 > *N* > 39; *3*, 63 > *N* > 67; *4*, 123 > *N* > 127. Globular structure.

this type of computer experiment allows us to carry out the corrections and transformations of the model and thereby to extend the scope of models including the formation of bi- and even polyheterometallic nanoparticles. Most likely, such improved and multiparametric models can be useful for optimization of metallopolymer nanocomposites.

Thus, thermal methods for synthesis of nanoparticles in a polymer matrix possess unlimited opportunities for the construction of polymer nanocomposites and for a choice of the optimal variant. In this chapter we did not analyze sol–gel synthesis of nanocomposites as well as hybrid polymer–inorganic nanocomposites, in preparation of which the controlled thermolysis plays an important role.

Many theoretical problems concerning physicochemistry of generation and growth of nanoparticles and the influence of polymer matrix on their composition and structure as well as the peculiarities of the growth of fractal and fractal filaments, specifics, and limitations of cluster–cluster aggregations are still necessary to solve. All these problems for polymer free nanostructures are mainly studied in detail and analyzed on the quantitative level. There have been attempts to clarify reactivity of the atomic metal regarding the polymer surface from the ionization potential of metal and the energy of low vacancy molecular orbital of polymer. The approaches based on the controlled pyrolysis to obtain polymer-mediated self-organized magnetic nanoparticles have been successfully developed. For example, magnetic materials on the base of binary FePt [130] obtained by thermal reduction of $Pt(AcAc)_2$ and $FeCl_2$ or CoPt [131] as well as PtRu [95] bimetallic nanoparticles are described. Recently, the synthesis of $Fe_{50}Pt_{50}$ using PVP or polyethyleneimine (PEI) [132] is performed. The multilayer self-assembled nanoparticles are localized on the PEI-modified silicon oxide surface. The optimal annealing time and temperature (30 min at 770–870 K) were found when the cubic form of a Pt nanoparticle transforms into hexagonal ones. Such layer-by-layer assembled nanoparticles possess the great potentials.

REFERENCES

1. A. D. Pomogailo, A. S. Rozenberg, and I. E. Uflyand, *Metal Nanoparticles in Polymers*, Khimiya, Moscow (2000), 672 pages.
2. M. J. Hampden-Smith and T. T. Kodas, *Chem. Vap. Deposition* **1**, 8 (1995).
3. A. D. Pomogailo and I. E. Uflyand, *Macromolecular Metal Chelates*, Khimiya, Moscow (1991).
4. E. I. Aleksandrova, G. I. Dzhardimalieva, A. S. Rozenberg, and A. D. Pomogailo, *Russ. Chem. Bull.* **42**, 259 (1993) (English translation).

5. E. I. Aleksandrova, G. I. Dzhardimalieva, A. S. Rozenberg, and A. D. Pomogailo, *Russ. Chem. Bull.* **42**, 264 (1993) (English translation).
6. Yu. M. Shulga, O. S. Roshchupkina, G. I. Dzhardimalieva, I. V. Chernushchevich, A. F. Dodonov, Yu. V. Baldokhin, P. Ya. Kolotyrkin, A. S. Rozenberg, and A. D. Pomogailo, *Russ. Chem. Bull.* **42**, 1661 (1993) (English translation).
7. A. S. Rozenberg, E. I. Alexandrova, G. I. Dzhardimalieva, A. N. Titkov, and A. D. Pomogailo, *Russ. Chem. Bull.* **42**, 1666 (1993) (English translation).
8. A. S. Rozenberg, E. I. Alexandrova, G. I. Dzhardimalieva, N. V. Kir'ykov, P. E. Chizhov, V. I. Petinov, and A. D. Pomogailo, *Russ. Chem. Bull.* **44**, 858 (1995) (English translation).
9. A. S. Rozenberg, G. I. Dzhardimalieva, and A. D. Pomogailo, *Polym. Adv. Technol.* **9**, 527 (1998).
10. S. Madorskii, *Thermal Decomposition of Organic Polymers*, Mir, Moscow (1967).
11. D. Wöhrle and A. D. Pomogailo, *Metal Complexes and Metals in Macromolecules: Synthesis, Structures and Properties*, Wiley-VCH, Weinheim (2003), 667 pages.
12. C. Paal and C. Amberger, *Ber. Dtsch. Chem. Ges.* **37**, 124 (1904).
13. A. D. Pomogailo and D. Wöhrle, in *Macromolecule–Metal Complexes*, edited by F. Ciardelli, E. Tsuchida, and D. Wohrle, Springer, Berlin (1996), pp. 11–129.
14. S. N. Zhurkov, V. A. Zakrevskii, V. E. Korsukov, and V. S. Kuksenko, *Phys. solids.* **13**, 2004 (1971).
15. G. M. Bartenev and E. S. Savin, *Polym. Sci. USSR. Ser. B* **25**, 625 (1982).
16. O. F. Shlenskii, N. V. Afanas'ev, and A. G. Shashkov, *Thermodestruction of Materials*, Energoatomizdat, Moscow (1996).
17. L. V. Ruban and G. E. Zaikov, *Russ. Chem. Rev.* **63**, 373 (1994).
18. R. S. Beer, C. A. Wilkie, and M. L. Mittleman, *J. Appl. Polym. Sci.* **46**, 1095 (1992).
19. I. C. McNeill and R. C. McGuiness, *Polym. Degrad. Stabil.* **9**, 1 (1984).
20. C. A. Wilkie, J. W. Pettergreww, and C. E. Brown, *J. Polym. Sci., Polym. Lett.* **19**, 409 (1981).
21. L. E. Manring, *Macromolecules* **21**, 528 (1988); **22**, 2673 (1989); **24**, 3304 (1991).
22. L. E. Manring, D. Y. Sogah, and G. M. Cohen, *Macromolecules* **22**, 4652 (1989).
23. C. A. Wilkie, J. T. Leone, and M. L. Mittleman, *J. Appl. Polym. Sci.* **42**, 1133 (1991).
24. K. Gurova, C. Uzov, M. Zagortcheva, and G. Gavrilova, *J. Appl. Polym. Sci.* **74**, 3324 (1999).
25. T.-H. Ko and C.-Y. Chen, *J. Appl. Polym. Sci.* **71**, 2219 (1999).
26. A. M. Summan, *J. Polym. Sci., Part A: Polym. Chem.* **37**, 3057 (1999).
27. L. Belfiore, M. P. McCurdie, and E. Ueda, *Macromolecules* **26**, 6908 (1993).

28. O. P. Krivoruchko and V. I. Zaikovskii, *Mendeleev Commun.* 97 (1998).
29. C. McNeill and J. J. Liggat, *Polym. Degrad. Stabil.* **29**, 93 (1990); **37**, 25 (1992).
30. S. P. Gubin and I. D. Kosobudskii, *Russ. Chem. Rev.* **52**, 1350 (1983).
31. N. M. Bravaya, A. D. Pomogailo, and E. F. Vainshtein. *Kinet. Catal.* **25**, 1140 (1984).
32. E. F. Vainshtein and G. E. Zaikov, in *Polymer Yearbook*, Vol. 10, edited by R. A. Pethric, Harwood Academic Publishers, London (1993), p. 231.
33. E. I. Aleksandrova, A. S. Rozenberg, and A. N. Titkiv, *Chem Phys.* **13**(8–9), 83 (1994).
34. D. Dollimore, *Thermochim. Acta* **117**, 331 (1987).
35. I. V. Kumpanenko and N. V. Chukanov, *Russ. Chem. Rev.* **50**, 1627 (1981).
36. A. D. Pomogailo, G. I. Dzhardimalieva, A. S. Rosenberg, and D. N. Muraviev, *J. Nanoparticle Res.* **5**, 497 (2003).
37. A. N. Timofeev, I. Yu. Filatov, V. G. Savostyanov, and K. I. Marushkin, *High Pure Substances* **5**, 45 (1994).
38. A. D. Pomogailo, A. S. Rozenberg, and G. I. Dzhardimalieva, in *Metal-Containing Polymers Materials*, edited by Ch. U. Pittman, Jr., Ch. E. Carraher, Jr., M. Zeldin, J. E. Sheats, and B. M. Culbertson, Plenum Press, New York, (1996), p. 313.
39. M. Ławecka, M. Leonowicz, M. Kopcewicz, A. Ślawska-Waniewska, J. Kozubowski, G. I. Dzhardimalieva, A. S. Rozenberg, and A. D. Pomogailo, *Kompozyty* (*Composites*) **2**, 404 (2002).
40. A. S. Rozenberg, E. I. Alexandrova, N. P. Ivleva, G. I. Dzhardimalieva, A. V. Raevskii, O. I. Kolesova, I. E. Uflyand, and A. D. Pomogailo, *Russ. Chem. Bull.* **47**, 259 (1998) (English translation).
41. A. T. Shuvaev, A. S. Rozenberg, G. I. Dzhardimalieva, N. P. Ivleva, V. G. Vlasenko, T. I. Nedoseikina, T. A. Lyubeznova, I. E. Uflyand, and A. D. Pomogailo, *Russ. Chem. Bull.* **47**, 1460 (1998) (English Translation).
42. I. Skupinska, H. Wilezura, and H. Bonink, *J. Therm. Anal.* **31**, 1017 (1986).
43. A. Gronowski and Z. Wojtezak, *J. Therm. Anal.* **36**, 2357 (1990).
44. P. A. Vasil'ev, A. L. Ivanov, and A. N. Glebov, *Russ. J. Gen. Chem.* **68**, 535 (1998).
45. A. S. Rozenberg, G. I. Dzhardimalieva, and A. D. Pomogailo, *Dokl. Phys. Chem.* **356**, 66 (1997).
46. A. D. Pomogailo, V. G. Vlasenko, A. T. Schuvaev, A. S. Rozenberg, and G. I. Dzhardimalieva, *Colloid J.* **64**, 524 (2002).
47. A. D. Pomogailo, A. S. Rozenberg, G. I. Dzhardimalieva, and M. Leonowicz, *Adv. Mater. Sci.* **1**, 19 (2001).
48. A. D. Pomogailo, G. I. Dzhardimalieva, and A. S. Rosenberg, *Acta Phys. Pol. A*, **102**, 135 (2002).
49. A. D. Pomogailo, A. S. Rosenberg, and G. I. Dzhardimalieva, *Solid State Phenom.* **94**, 313 (2003).
50. V. A. Sergeev, N. I. Bekasiova, M. A. Surikova, E. A. Baryshnikova, Ya. V. Genin, and N. K. Vinogradova, *Dokl. Phys. Chem.* **332**, 601 (1993).

51. V. A. Sergeev, N. I. Bekasov, and M. A. Surikova, *Polym. Sci. Ser. B* **34**, 70 (1992).
52. V. G. Syrkin, *Gas-Phase Metallization Through Carbonyls*, Metallurgy, Moscow (1985).
53. T. W. Smith and D. Wychick, *J. Phys. Chem*. **84**, 1621 (1980).
54. Patent 4252671-4252678, CIIIA.
55. P. H. Hess and P. H. Parker, Jr., *J. Appl. Polym. Sci*. **10**, 1915 (1966).
56. J. R. Thomas, *J. Appl. Phys.* **37**, 2914 (1966).
57. M. Berger and T. A. Manuel, *J. Polym. Sci.* A-1 **4**, 1509 (1966).
58. T. W. Smith and D. J. Luca, *Proceedings, Symposium on Modified Polymers, Las Vegas (Nev.) 1982*. Abstract New York, London (1983), p. 85.
59. A. B. Gilman and V. M. Kolotyrkin, *High Energy Chem.* **12**, 450 (1978).
60. C. H. Griffiths, M. P. O'Horo, and T. W. Smith, *J. Appl. Phys*. **50**, 7108 (1979).
61. H. Biederman, *Vacuum* **34**, 405 (1984).
62. C. E. Kerr, B. E. Eaton, and J. A. Kadue, *Organometallics* **14**, 269 (1995).
63. S. P. Gubin, I. D. Kosobudskii, and G. I. Petrakovskii, *Dokl. AN USSR* **260**, 655 (1981).
64. S. P. Gubin and I. D. Kosobudskii, *Dokl. AN USSR* **272**, 1155 (1983).
65. I. D. Kosobudskii, S. P. Gubin, V. P. Piskorskii, G. A. Petrakovskii, L. V. Kashkina, V. N. Kolomiichuk, and N. M. Svirskaya, in *Electronics of Organic Materials*, edited by A. A. Ovchinnikov, Nauka, Moscow (1985), p. 62.
66. L. M. Bronshtein, P. M. Valetskii, S. V. Vinogradova, A. I. Kuzaev, and V. V. Korshak, *Polym. Sci. USSR* **29**, 1694 (1987).
67. C. U. Pittman, Jr, P. L. Grube, O. E. Ayers, S. P. McManus, M. D. Rausch, and G. A. Moser, *J. Polym. Sci.*, A-1, **10**, 379 (1972).
68. L. M. Bronstein, S. P. Solodovnikov, E. Sh. Mirzoeva, E. Yu. Baukova, and P. M. Valetsky, *Proc. ACS Div. Polym. Mater. Sci. Eng*. **71**, 397 (1994).
69. M. Berger and D. J. Buckley. *J. Polym. Sci*., A-1, **1**, 2945 (1963).
70. R. A. Arents, Yu. V. Maksimov, I. P. Suzdalev, and Yu. B. Amerik, *Hyperfine Interactions*, **56**, 167 (1990).
71. Yu. B. Amerik, Yu. M. Korolev, and V. N. Rogovoi, *Neftekhimiya*, **36**, 304 (1996).
72. Yu. M. Korolov, A. L. Bykova, and Yu. B. Amerik, *Polym. Sci. Ser. B*, **39**, 1856 (1997).
73. P. I. Dosa, C. Erben, V. S. Iyer, K. P. C. Vollhard, and I. M. Vasser, *J. Am. Chem. Soc*. **121**, 10430 (1999).
74. C.-H. Kiang and W. A. Goddard, *Phys. Rev. Lett.* **76**, 2515 (1996).
75. R. Sen, A. Govindaraj, and C. N. R. Rao, *Chem. Mater.* **9**, 2078 (1997).
76. T. X. Neenan, M. R. Callstrom, and O. J. Schueller, *Macromol. Symp*. **80**, 315 (1994).
77. F. Galembeck, C. C. Chironi, and C. A. Ribeiro, et al. *J. Appl. Polym. Sci*. **25**, 1427 (1980).

78. R. Baumhardt-Neto, S. E. Galembeck, I. Joekes, and F. Galembeck, *J. Polym. Sci., Polym. Chem. Ed.* **19**, 819 (1981).
79. F. Galembeck, *J. Polym. Sci.: Polym. Lett. Ed.* **15**, 107 (1977); *J. Polym. Sci.: Polym. Chem. Ed.* **16**, 3015 (1978).
80. R. Tannenbaum, C. L. Flenniken, and E. P. Goldberg, in *Metal-Containing Polymeric Systems*, edited by C. Carraher, C. Pittman, and J. Sheats, Plenum, New York (1985), p. 303.
81. R. Tannenbaum, C. L. Flenniken, and E. P. Goldberg, *J. Polym. Sci.: Part B: Polym. Phys.* **28**, 2421 (1990).
82. S. Reich and E. P. Goldberg, *J. Polym. Sci., Phys. Ed.* **21**, 869 (1983).
83. A. I. Pertsin and Yu. M. Poshutin, *Polym. Sci. Ser. B* **38**, 919 (1996).
84. A. I. Pertsin and I. O. Volkov, *Polym. Sci. Ser. B* **38**, 1249 (1996).
85. L. M. Bronshtein, P. M. Valetskii, and M. Antonietti, *Polym. Sci. Ser. A* **39**, 1847 (1997).
86. O. A. Platonova, L. M. Bronstein, S. P. Solodovnikov, I. M. Yanovskaya, E. S. Obolonkova, P. M. Valetsky, E. Wenz, and M. Antonietti, *Colloid Polym. Sci.* **275**, 426 (1997).
87. K. S. Suslick (editor). *Ultrasound: Its Chemical, Physical, and Biological Effects*, VCH Press, New York (1988).
88. K. S. Suslick, *Science* **247**, 1439 (1990).
89. K. S. Suslick, S. B. Choe, A. A. Cichowlas, and M. W. Grinstaff, *Nature* **353**, 414 (1991).
90. G. Kataby, T. Prozorov, Yu. Koltyp, C. N. Sukenik, A. Ulman, and A. Gedanken, *Langmuir* **13**, 615 (1997); **15**, 1702 (1999).
91. K. V. P. M. Shafi, A. Gedanken, R. Prozorov, and J. Balogh, *Chem. Mater.* **10**, 3445 (1998).
92. K. S. Suslick, T. Hyeon, M. Fang, and A. A. Cichowlas, *Mater. Sci. Eng.* **A204**, 186 (1996); *Chem. Mater.* **8**, 2172 (1996).
93. D. Caro, T. O. Ely, A. Mari, B. Chaudret, E. Snoeck, M. Respaud, J.-M. Broto, and A. Fert, *Chem. Mater.* **8**, 1987 (1996).
94. K. V. P. M. Shafi, A. Ulman, X. Yan, N.-L. Yang, C. Estournes, H. White, and M. Rafailovich, *Langmuir* **17**, 5093 (2001).
95. M. S. Nashner, A. I. Frenkel, D. Somerville, C. W. Hills, J. R. Shapley, and R. G. Nuzzo, *J. Am. Chem. Soc.* **120**, 8093 (1998).
96. T. Yu. Ryabova, A. S. Chirkov, L. S. Radkevich, and N. V. Evtushok, *Ukr. Chem. J.* **59**, 1329 (1993).
97. A. I. Savitskii, Sh. Ya. Korovskii, and V. I. Prosvirin, *Colloid J. USSR*, **41**, 88 (1979); **42**, 998 (1980).
98. M. C. Alves and G. Tourillon, *J. Phys. Chem.* **100**, 7566 (1996).
99. J. E. Millburn and M. J. Rosseinsky, *Chem. Mater.* **9**, 511 (1997).
100. R. E. Southward, D. W. Thompson, and A. K. St. Clair, *Chem. Mater.* **9**, 501 (1997).

101. R. E. Southward, D. S. Thompson, D. W. Thompson, and A. K. St. Clair, *Chem. Mater.* **9**, 1691 (1997).
102. S. P. Pogorelov, G. M. Plavnik, A. P. Tikhonov, and T. P. Puryaeva, *Colloid J.* **61**, 100 (1999).
103. Yu. M. Khimchenko and L. S. Radkevich, *Plast. Massy* **1**, 53 (1975).
104. N. I. Nikanorova, E. S. Trofimchuk, E. V. Semenova, A. L. Bolynskii, and N. F. Bakeev, *Polym. Sci. Ser. A* **42**, 1298 (2000).
105. G. Carotenuto, B. Martorana, P. Perlo, and L. Nicolais, *J. Mater. Chem.* **13**, 2927 (2003).
106. A. Yu. Vasilkov, P. V. Pribytko, E. A. Fedorovskaya, A. A. Slinkin, A. S. Kogan, and V. A. Sergeev, *Dokl. Phys. Chem.* **331**, 179 (1993).
107. J. Osuna, D. Caro, C. Amiens, B. Chaudret, E. Snoeck, M. Respaund, J.-M. Broto, and A. Fest, *J. Phys. Chem.* **100**, 14571 (1996).
108. A. Carbonaro, A. Greco, and G. Dall'asta, *J. Organomet. Chem.* **20**, 177 (1969).
109. S. E. J. Goff, T. F. Nolan, M. W. George, and M. Poliakoff, *Organometallics* **17**, 2730 (1998).
110. A. I. Cooper and M. Poliakoff, *Chem. Phys.* Lett. **212**, 611 (1993).
111. J. S. Bradley, J. M. Millar, E. W. Hill, S. Behal, B. Chaudret, and A. Duteil, *Faraday Discuss. Chem. Soc.* **92**, 255 (1991).
112. A. Duteil, R. Queau, B. M. Chaudret, C. Roucau, and J. S. Bradley, *Chem. Mater.* **5**, 341 (1993).
113. J. S. Bradley, E. W. Hill, S. Behal, C. Klein, B. M. Chaudret, and A. Duteil, *Chem. Mater.* **4**, 1234 (1992).
114. D. Caro and J. S. Bradley, *Langmuir* **13**, 3067 (1997).
115. F. Waller, *J. Catal. Rev. Sci. Eng.* **28**, 1 (1986).
116. A. M. Hodges, M. Linton, A. W.-H. Mau, K. J. Cavell, J. A. Hey, and A. Seen, *J. Appl. Organomet. Chem.* **4**, 465 (1990).
117. M. Pehnt, D. L. Schulz, C. J. Curtis, K. M. Jones, and D. S. Ginley, *Appl. Phys. Lett.* **67**, 2176 (1995).
118. E. E. Said-Galeev, L. N. Nikitin, Yu. P. Kudryavtsev, A. L. Rusanov, O. L. Lependina, V. K. Popov, M. Polyakoff, and S. M. Houdl, *Khim Phizika*, **14**, 190 (1995).
119. J. J. Watkins and T. J. McCarthy, *Chem. Mater.* **7**, 1991 (1995).
120. J. J. Watkins and T. J. McCarthy, *Polym. Mater. Sci. Eng.* **73**, 158 (1995).
121. E. M. Natanson and Z. P. Ulberg, *Colloid Metals and Metallopolymers*, Naukova Dumka, Kiev (1971).
122. D. M. Mognonov, V. G. Samsonova, V. V. Khakinov, and I. N. Pinchuk, *Polym. Sci. Ser. B* **39**, 1250 (1997).
123. G. P. Gladyshev, O. A. Vasnetsova, and N. I. Mashukov, *Mendeleev. Chem. J.* **34**, 575 (1990).
124. G. P. Gladyshev, N. I. Mashukov, and S. A. Eltsin, *Polym. Sci. USSR, B* **28**, 62 (1986).

125. N. D. Zhuravlev, V. I. Raldugin, and A. P. Tikhonov, *Colloid J.* **61**, 322 (1999).
126. S. Kan, S. Yu, and X. Peng, *J. Colloid. Interface Sci.* **178**, 673 (1966).
127. A. S. Rozenberg, A. A. Rozenberg, G. I. Dzhardimalieva, and A. D. Pomogailo, in *Program and Abstracts, 10th IUPAC Internernational Symposium on Macromolecule–Metal Complexes, Moscow, May 18–23, 2003*, edited by E. A. Karakhanov and A. L. Maximov, MAX Press, Moscow (2003), p. 101.
128. D. E. Ulberg, V. V. Il'in, N. V. Churaev, and Yu. V. Nizhnik, *Colloid J.* **54**, 151 (1992).
129. A. S. Roseberg, A. A. Rosenberg, A. V. Lankin, G. I. Dzhardimalieva, and A. D. Pomogailo, *Dokl. Phys. Chem.* **393**, 361 (2003).
130. S. Sun, C. B. Murray, D. Weller, L. Folks, and A. Moser, *Science*, **287**, 1989 (2000).
131. J. H. Park and J. Cheon, *J. Am. Chem. Soc.* **123**, 5473 (2001).
132. S. Sun, S. Anders, H. F. Haman, J.-U. Thiele, J. E. E. Baglin, T. Thomson, E. E. Fullerton, C. B. Murray, and B. D. Terris, *J. Am. Chem. Soc.* **124**, 2884 (2002).